Precambrian Research 368 (2022) 106479

Contents lists available at ScienceDirect

Precambrian Research

journal homepage: www.elsevier.com/locate/precamres

Contrasting *P-T*-t paths of basement and cover within the Búzios Orogen, SE Brazil – Tracking Ediacaran-Cambrian subduction zones

Thayla Almeida Teixeira Vieira [a,*], Renata da Silva Schmitt [a,b], Julio Cezar Mendes [a,b], Renato Moraes [c], George Luiz Luvizotto [d], Raphaela Lopes de Andrade Silva [b], Rodrigo Vinagre [a,b], Silvia Regina de Medeiros [a,b]

[a] *Programa de Pós-Graduação em Geologia – PPGL – IGEO, Universidade Federal do Rio de Janeiro, UFRJ, Athos da Silveira Ramos Avenue, 274, block G – Cidade Universitária, Ilha do Fundão, CEP: 21941-916 Rio de Janeiro, RJ, Brazil*
[b] *Departamento de Geologia – IGEO, Universidade Federal do Rio de Janeiro, Rio de Janeiro, Brazil*
[c] *Departamento de Mineralogia e Geotectônica, Instituto de Geociências, Universidade de São Paulo, São Paulo, Brazil*
[d] *Departamento de Geologia, Universidade Estadual Paulista, São Paulo, Brazil*

ARTICLE INFO

Keywords:
Cabo Frio Tectonic Domain
Geothermobarometry
Petrochronology
U-Pb zircon
U-Pb-Th monazite
Zr-in-rutile

ABSTRACT

Deeply eroded collisional orogens show complex structural and inverted stratigraphic relations with juxtaposition of rock stacks from distinct crustal levels, origins and ages, hence with contrasting *P-T*-t paths during convergent tectonics. This paper presents petrochronological data on Paleoproterozoic (basement) and Ediacaran (cover) gneisses tectonically interleaved during the Ediacaran-Cambrian Búzios Orogeny, in southeastern Brazil. U-Pb in zircon and EPMA U-Th-Pb in monazite data, coupled with geothermobarometric data, plus Zr-in-rutile, reveal that at a first orogenic stage (ca. 530–520 Ma), these units were at distinct crustal levels. Samples within the Paleoproterozoic basement show metamorphic near-peak conditions of ~800 °C and 10 kbar, at a depth of c.37 km. Contrastingly, Ediacaran kyanite-orthoclase-garnet-biotite granulite with retrometamorphic sillimanite (cover) reached near-peak conditions of 15 kbar and 818 °C–785 °C at depths of c. 55 km, in high-pressure granulite facies. This deep burial of Ediacaran sediments in less than 20 m.y. would be compatible with a low angle subduction zone active from ca. 550 to 530 Ma. Intrusion of ca. 550 Ma tholeiitic dykes in the Paleoproterozoic gneiss indicates a high geothermal gradient for this subduction setting, which is consistent with a low subduction rate. In a second orogenic stage (ca. 520–500 Ma), these distinct stratigraphic units were placed tectonically side by side during a fast exhumation, preserving an inverted metamorphic stack. The cover underwent retrometamorphic conditions of 800 °C and 10 kbar on a clockwise return path due to decompression. It is proposed here that the contact between reworked units within a Paleoproterozoic continental crust and Ediacaran magmatic and sedimentary units represent the suture of an Ediacaran NW-subduction of the Angola continental paleomargin below the Oriental Terrane of the Ribeira belt. This paper reports the highest pressure recorded in Ediacaran-Cambrian metamorphic rocks from the Brasiliano belts along the actual South Atlantic continental margins. The suture we propose here is aligned along strike, with a medium to high-pressure Ediacaran metamorphic occurrence 700 km to the SW, in the Curitiba Terrane.

1. Introduction

Deeply eroded collisional orogens expose complex structural relationships due to evolution of deformation and metamorphism during convergent tectonics (Butler 2018; Donaldson et al., 2013; Möller et al., 2018; Moraes et al., 2002). The final result may present inverted stratigraphic relations, with juxtaposition of rock stacks originated from distinct crustal levels with diverse *P-T*-t paths (Campos Neto, 2000; Coelho et al., 2017; Treloar et al., 2019; Trouw et al., 2000). In addition, the collisional metamorphic event may obliterate earlier *P-T* conditions that might be related to partial subduction or to a thermal effect of the magmatic arc.

Inliers of older continental crust within the orogenic belts are key to unravel the *P-T*-t trajectories since they undergo the entire orogenic

* Corresponding author.
E-mail address: thaylalmeida@gmail.com (T.A.T. Vieira).

https://doi.org/10.1016/j.precamres.2021.106479
Received 2 March 2021; Received in revised form 30 August 2021; Accepted 12 November 2021
Available online 8 December 2021

evolution. However, these basement units configure an extra challenge because they might have been affected by other orogenic cycles (Brito Neves et al., 2014; Herwegh and Pfiffner, 2005). Within the internal orogenic belt this ancient basement is tectonically interleaved with early to *syn*-orogenic rock units. The contrasting age, *P-T*-t paths and origins are crucial characteristics to allow the understanding of the geodynamic evolution of a collisional belt.

Geothermobarometric studies allied with geochronological data, assist in the quantification of the metamorphic conditions through time (Rubatto, 2002, 2017; Tedeschi et al., 2017). Furthermore, the combination of zircon and monazite U-Th-Pb geochronology preserves the timing of orogenic events due to their chemical stability and high closure temperatures (Cherniak and Watson, 2001). By linking zircon and monazite growth it is possible to obtain a direct assessment of the timing of tectono-metamorphic events (Rocha et al., 2017; Rubatto et al., 2001).

This paper presents petrochronological data on metamorphic rocks from a 1.5 km detailed geological cross section along the southeastern Brazilian coast in the context of the Central Ribeira belt. This is a key area to investigate the *P-T*-t paths of Paleoproterozoic and Neoproterozoic gneisses tectonically interleaved during a Cambrian collisional event (Schmitt et al., 2004, 2016). By dating U-Pb in zircon and U-Th-Pb in monazite, coupled with geothermobarometric studies in samples from basement and cover units, we provide new tectonic insights for evolution of the Ribeira belt, testing alternative approaches to investigate deeply eroded and poorly exposed collisional orogens. In addition, we judge the hypothesis that the paragneisses correlated with the Búzios Succession were buried to great depths, providing evidence to track subduction zones that led to Gondwana amalgamation.

2. Tectonic setting

The NE-SW Ribeira Belt is a product of the convergence and collision between São Francisco-Congo (Alkmim et al., 2006), Angola and Paranapanema cratons (Heilbron et al., 2008), and some microplates (e.g., Serra do Mar – Campos Neto and Figueiredo, 1995) from the Ediacaran to the lower Paleozoic (Fig. 1a – Schmitt et al., 2018). The Ribeira Belt extends to the north merged with the coeval Araçuaí Belt, and to the south it is in contact with the Luis Alves Craton (Fig. 1a – Heilbron et al., 2004, Schmitt et al., 2018). To the west it partly overlaps the 50 m.y. older Brasilia Belt producing an interference zone (Trouw et al., 2013).

Its central portion is divided in four tectonic domains (Fig. 1a – Heilbron et al., 2000; Heilbron et al., 2008). The western part comprises the Occidental Terrane and the Paraíba do Sul/Embu Terrane. These terranes have basement units from the São Francisco and the Paranapanema cratons, which were reworked, but only the former was tectonically intercalated with continental margin sedimentary rocks (dark green in Fig. 1a). The Oriental Terrane and the Cabo Frio Tectonic Domain constitute the eastern segment, both detailed below (lighter greens in Fig. 1a, detail in Fig. 1b.

The Oriental Terrane is comprised of high T – low P supracrustal units intruded by pre-collisional plutons interpreted as three magmatic arcs (Serra da Bolivia, 859–838 Ma, Heilbron et al., 2013; Serra da Prata, 790–620 Ma, Peixoto et al., 2017; and Rio Negro arcs, 650–585 Ma, Tupinambá et al., 2012), and by syn- to post-collisional plutons (580–460 Ma; Heilbron and Machado, 2003; Martins et al., 2016; Mendes et al., 2006; Silva et al., 2003; Valeriano et al., 2011). According to Heilbron et al. (2004), the contact between the Occidental and Oriental terranes is a suture zone, generated during the SE subduction of the São Francisco continental paleomargin (Fig. 1a). In this scenario, the Oriental Terrane would represent the upper plate consistent with the magmatic arc setting at a high T – low P regime. These authors propose a 580 Ma collision between the arc-domain (Oriental Terrane) and the continental margin, to the NW. No basement rocks older than the Neoproterozoic have been reported from the Oriental Terrane.

To the southeast, along the Rio de Janeiro coast, the Neoproterozoic Oriental Terrane has a sharp tectonic contact with the Cabo Frio Tectonic Domain (CFTD – Fig. 1b and 2). The latter, focus of this study, is predominantly composed of Paleoproterozoic orthogneisses correlated with the African Angola craton (Região dos Lagos Complex – Fig. 1a; De Waele et al., 2008; Delor et al., 2006; Monié et al., 2012; Schmitt et al., 2016). It is tectonically interleaved with Ediacaran high *P-T* paragneisses and metabasites. The metamorphic ages are at least 50 m.y. younger than the Oriental Terrane, and are attributed to the collision, between the Angola continental paleomargin and the Oriental Terrane (Cambrian Búzios Orogeny – Fig. 1a, Schmitt et al., 2004). Heilbron and Machado (2003) interpreted this event as a response to the closure of a back-arc basin related to the Rio Negro magmatic arc of the Oriental Terrane. Other authors propose that the contact between the Oriental Terrane and the Cabo Frio Tectonic Domain is a suture due to a NW-directed subduction zone (Capistrano et al., 2017; Capistrano et al., 2020; Fernandes et al., 2015; Martins et al., 2016; Schmitt et al., 2008; Schmitt et al., 2016). In this interpretation, the supracrustal units of the Cabo Frio Tectonic Domain would represent forearc and accretionary prism sequences and not back-arc sediments. The metamorphic conditions and *P-T* path of the Búzios Succession and the tectonically interleaved Região dos Lagos Complex may provide evidence to better constrain the geodynamic evolution of this belt. Additionally, there are alternative tectonic models which consider an intracontinental orogenic belt without the subduction of oceanic crust recently proposed in the literature (Fossen et al., 2020; Meira et al., 2015; Meira et al., 2019; Meira et al., 2020).

2.1. Geological units of the Cabo Frio Tectonic Domain

The Cabo Frio Tectonic Domain (CFTD) is composed of three main lithostratigraphic units: Paleoproterozoic orthogneisses (Região dos Lagos Complex – Fonseca et al., 1979) and two Ediacaran supracrustal sequences (Búzios and Palmital Successions, Fig. 1b – Schmitt et al., 2008). The orthogneisses are predominantly granitic/granodioritic with subordinate diorites, representing a calc-alkaline magmatic series of Orosirian age (ca. 2.0–1.94 Ga – Schmitt et al., 2004, 2008b, 2016; Viana et al., 2008), cross cut by 5–15-meter-thick amphibolite bodies (José Gonçalves suite, Schmitt et al., 2009), former diabase bodies. No supracrustal or igneous rocks older than this plutonic complex were recognized so far, only inherited 2.6 – 2.5 Ga zircon cores (Schmitt and Armstrong, 2014).

The Ediacaran supracrustal units include aluminous gneisses, psammitic gneisses, calc-silicate rocks, and metabasites (Schmitt et al., 2004), separated in two successions: Palmital and Búzios (Fig. 1b – Schmitt et al., 2004; Schmitt et al., 2008). The former occurs along the contact between the CFTD and the Oriental Terrane and also as a klippe in the CFTD (Fig. 1b). The Palmital Succession is interpreted as a fore arc sedimentary succession deposited between 560 and 530 Ma, according to U-Pb ages of detrital and metamorphic zircon (Capistrano et al., 2017; Capistrano et al., 2020; Fernandes et al., 2015), with litharenitic protolith (Capistrano et al., 2017; Fernandes et al., 2015). The predominant detrital zircon population from the Palmital Succession varies between 700 and 600 Ma and the maximum deposition age for this succession is 566 ± 9 Ma (Fernandes et al., 2015).

The Búzios Succession, located only in the coastal region (Fig. 1b), comprises metamorphic rocks with deep-sea sedimentary and volcanic protoliths formed between 600 and 550 Ma in an oceanic crust realm, incorporated into the accretionary prism during convergent tectonics (Capistrano et al., 2020; Schmitt et al., 2008). U-Pb data on aluminous gneisses from the Búzios Succession revealed a major Ediacaran detrital zircon population, with ca. 583 Ma as a maximum age of deposition, and with a metamorphic overprint at ca. 521 ± 11 Ma dated in zircon rims (Capistrano et al., 2020).

Finally, both successions were deformed and metamorphosed during the transition from Ediacaran to Cambrian, under upper amphibolite (Palmital Succession) to medium- to high-pressure granulite facies

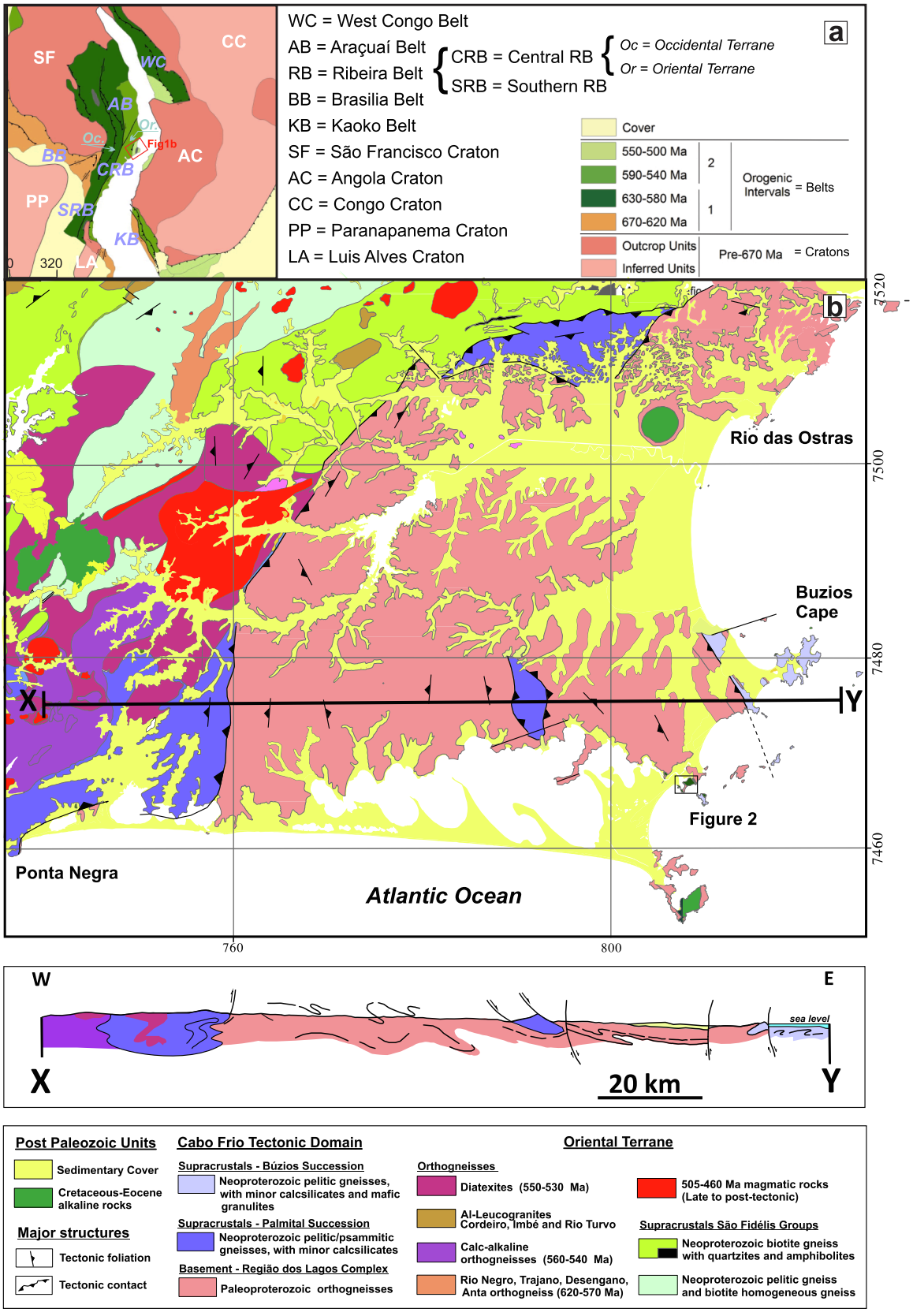

Fig. 1. (a) West Gondwana reconstructed including South America and Africa, with cratons and mobile belts shown. Red rectangle indicates location of Fig. 1b. Modified from Schmitt et al., 2018); (b) Simplified geological map of the Cabo Frio Tectonic Domain and eastern Oriental Terrane with E-W geological cross section. Modified from Schmitt et al. (2016) and Capistrano et al. (2020).

conditions (Búzios Succession) with widespread migmatization (Schmitt et al., 2004). Based on zircon, monazite, titanite and rutile dating, a rapid cooling curve of 20 °C/m.y. from 518 to 505 Ma was calculated for the Búzios paragneisses, recording a relatively fast exhumation of these deep-seated rock units (Schmitt et al., 2004). The interleaved Paleoproterozoic orthogneiss is also affected by this tectono-metamorphic event, with migmatitic zones concentrated along shear zones. Metamorphic conditions for the Região dos Lagos Complex were originally considered to follow the Búzios Succession *P-T*-t path (Schmitt et al., 2004), although some incompatibilities can be pointed out: (a) the strain and partial melt localization is observed only in the Paleoproterozoic basement; (b) the highly sheared contacts between the Paleoproterozoic orthogneiss and Búzios Succession; (c) the distinct protoliths (continental and oceanic crusts). In this paper, we will investigate this issue.

3. Methodology

3.1. Mineral chemistry

Amphibole, pyroxene, garnet, biotite, K-feldspar and plagioclase were analyzed for major elements in three thin sections (TH-5A, TH-10A and TH-34C) at the Electron Microprobe Laboratory (LABSONDA) of the Federal University of Rio de Janeiro (UFRJ) using a JEOL EPMA – JXA-8230 Electron Probe Micro-analyzer. The microprobe was operated in wavelength-dispersion system with five spectrometers and a set of eight analyzer crystals. Analytical conditions were accelerating voltage of 15 kV, sample current of 20 nA and beam diameter of 5 and 10 μm. International certificate standards of natural minerals, for equipment calibration and quantitative analyses, are either from the Smithsonian Institute – USA or from Astimex Scientific Limited, Serial KM, MINM 25–53.

Composition profiles were obtained in garnet and plagioclase, with five to ten spot analyses to verify variations between cores and rims. At least three crystals in five different fields on the same thin section were analyzed.

3.2. Monazite and rutile chemistry and U-Th-Pb dating

Monazite and rutile were analyzed in two thin sections (TH-10A and TH-34C) at the Department of Geology of the State University of São Paulo – UNESP. Analyses were carried out through wavelength dispersive spectrometry (WDS) using a JEOL JXA-8230 Electron Microprobe equipped with five WDS detectors. Monazite dating (U-Th-Pb) followed the instructions of Williams et al. (2006) and Vlach (2010). On the selected monazite grains, high resolution compositional X-ray maps were collected for Y, Th, U and Ca (15 kV, 100 nA, 100 s dwell time and 10 μm electron beam size and step). For the purpose of comparing concentration levels and zoning features, X-ray maps generated for crystals from the same sample were processed together using the identical color scale, i.e., same minimum and maximum magnitude values for all grains. The maps were then used to select different domains for U-Th-Pb spot analyses and later age calculations. Differently from the procedure highlighted by Williams et al. (2006), background measurements were performed for all analyses. Spot analyses were carried out using 15 kV, 100 nA, using background positions and PHA settings presented by Vlach (2010). To assess data quality, every 10 to 15 undetermined analyses were bracketed by three analyses on the Moacir monazite secondary standard (Paraíso monazite reported by Gonçalves et al., 2016) which are presented in the Supplementary Table 4. Spectral interference corrections (Th on U Pb and Th + Y on Pb Ma) were done offline and considered matrix correction factors. Interference corrections and age calculations were accomplished using the Age_Cor program (Vlach, 2010). Errors presented for each single spot and age were calculated using the 2-sigma relative standard errors (counting statistics) from the Electron Microprobe analyses. Data reduction was carried out using the software ISOPLOT 4 (Ludwig, 2009). Errors presented for multiple analyses (weighted mean) took into consideration error propagation and were calculated using the ISOPLOT 4 software (Ludwig, 2009).

Analyses of trace elements in rutile used a focused beam at 20 kV and 100 nA, following the method outlined by Luvizotto et al. (2009) and with the conditions presented in Table 1. Si, Al, Cr, Fe, Nb, Ti, and Zr were measured and Si concentrations were used as a quality control to detect contaminations, that is, analyses with Si concentration higher than 300 ppm were discarded from the data set. Analyses of the R10 rutile reference material (Luvizotto et al. 2009) are shown in Supplementary Table 3, and they were carried out after 15 unknown analyses to ensure the quality and reproducibility of the data. Zr-in-rutile temperatures were calculated with the calibration of Tomkins et al. (2007). Errors presented in temperature results were calculated using the 2-sigma relative standard errors (counting statistics) from the Electron Microprobe analyses.

3.3. U-Pb analyses on zircon

Zircon grains were separated from fresh crushed samples using conventional methods, heavy liquids and magnetic techniques (jaw crusher, disk grinder, Wilfley table, Frantz isodynamic magnetic separator and density separation using methylene iodide) at the Geological Laboratory of Samples Preparation (LGPA) at the State University of Rio de Janeiro (UERJ). Circa of 50–180 zircon grains from each sample were mounted in epoxy resin, polished to half of mean grain thickness for further imaging. The zircon grains were imaged in the Scanning Electron Microscope (SEM) model Quanta 250, Termo Scientific at MultiLab, at the Rio de Janeiro State University (UERJ) to unravel internal complexities with cathodoluminescence. SEM analytical conditions were: high voltage of 15 kV, work distance 16.9 mm, detector PMD, filament emission of 100 μA, and magnification range 95 to 250x. The U-Pb analyses were performed on samples (TH-34C) at MultiLab/UERJ. The laboratory has a multicollector Thermo (Neptune plus) coupled plasma induction mass spectrometer, ICP-MC-MS, and a laser ablation, Photon Machines, 193 mm. Isotopic data were obtained using the static mode through 40 cycles of 1.054 s acquirement time with a gas inlet flow (Ar) of 15 L / min, auxiliary flow (Ar) 0.90 L / min, in MC-ICP-MS. The laser a gas inlet He flow (two input streams with volumes of 0.700 / m and 0.220 / m). Repetition of the laser was at 6 Hz, with 4–7 J / cm^2 (35–60%) output power and 40–50 μm crater size. The acquisition method comprises of a sequence, that starts with the analysis of one blank, which is the measurement of the data performed of the passageway of only Ar and He gases, being measured as a background, followed by the mensuration of a shot made on a zircon primary standard (GJ-01). If the data are compatible with the genuine value described by Elhlou et al. (2006) ($^{206}Pb/^{207}Pb = 0.06389$ and $^{206}Pb/^{238}U = 0.09812$), thus the analysis of 9 grains of indefinite age can be done. After performing the undetermined analyses, data of another zircon secondary standard (91500, Wiedenbeck et al., 1995) is acquired, finalizing the spreadsheet with the reading of a second spot from GJ-1 (zircon standard) and a blank over again. The U-Pb results attained by

Table 1
Electron microprobe conditions applied for the monazite and rutile trace elements analysis.

20 kV / 80 nA	Si	Al	Cr	Fe	Ti	Nb	Zr
Crystal	TAP	TAP	PET	LIF	PET	PET	PET
Line	*Kα*	*Kα*	*Kα*	*Kα*	*Kβ*	*Lα*	*Lα*
Peak sec[a]	300	300	150	150	30	300	300
Bkg sec[b]	150	150	50	50	15	150	150
DL[c]	25	20	50	40	55	40	45

a Count time on peak position in seconds; *b* Count time on background position in seconds; *c* 2 σ detection limit, based on repeated measurement of variation on background, values in ppm.

LA-ICP-MS were treated in an offline spreadsheet for blank and GJ-01 correction. The Supplementary Table 1 contain the U-Pb analytical data acquired by the LA-ICP-MS. The program ISOPLOT was used to calculate ages and construct concordia diagrams (Ludwig, 2009) and decay constant values used are recommend by Steiger and Jäger (1977). All calculated values in the concordia and discordia diagrams are referred to 2σ for all uncertainties quoted in the body of the text.

U-Pb dating of sample TH-5A was analyzed by a Sensitive High-mass Resolution Ion MicroProbe (SHRIMP-II) at the Geochronological Research Center of the University of São Paulo (CPGeo-USP). The analysis was carried out with a spot size of 24 μm, analyzing grain rims and cores. Supplementary Table 2 includes the U-Pb analytical data acquired by the SHRIMP. The TEMORA 2 referenced standard was placed together in the mount – 4 zircon grains were used ($^{206}Pb/^{238}U$ age = 416.78 ± 0.33 Ma; Black et al., 2004). The analytical procedures, acquisition, and data processing were done following Sato et al. (2014). Correction for common Pb was made based on the measured ^{204}Pb, and the typical uncertainty component for the $^{206}Pb/^{238}U$ ratios is lesser than 2 percent. Data were reduced using SQUID 1.06 software, and Concordia age calculations were performed using the software ISOPLOT 4 (Ludwig, 2009). Data-point uncertainty ellipses in the Concordia and Discordia diagrams have two sigma of confidence level for all uncertainties quoted in the body of the text. The decay constant values used are recommend by Steiger and Jäger (1977).

4. Results

4.1. Geology of the area and studied samples

The studied area is a well-exposed 1.5 km geological section along the coast of Cabo Frio city with Paleoproterozoic (Região dos Lagos Complex) and Ediacaran gneisses (Búzios Succession) tectonically interleaved presenting high grade mineral paragenesis and local migmatization (Fig. 1b and 2). The main NW-SE tectonic foliation in both units shows medium to high dip, with subhorizontal mineral and stretching lineation. At least two coaxial folding phases were detected: isoclinal F2 folds and open recumbent to upright F3 folds (Fig. 2). Leucosome veins are folded by F2 and also intrude parallel to F2 and F3

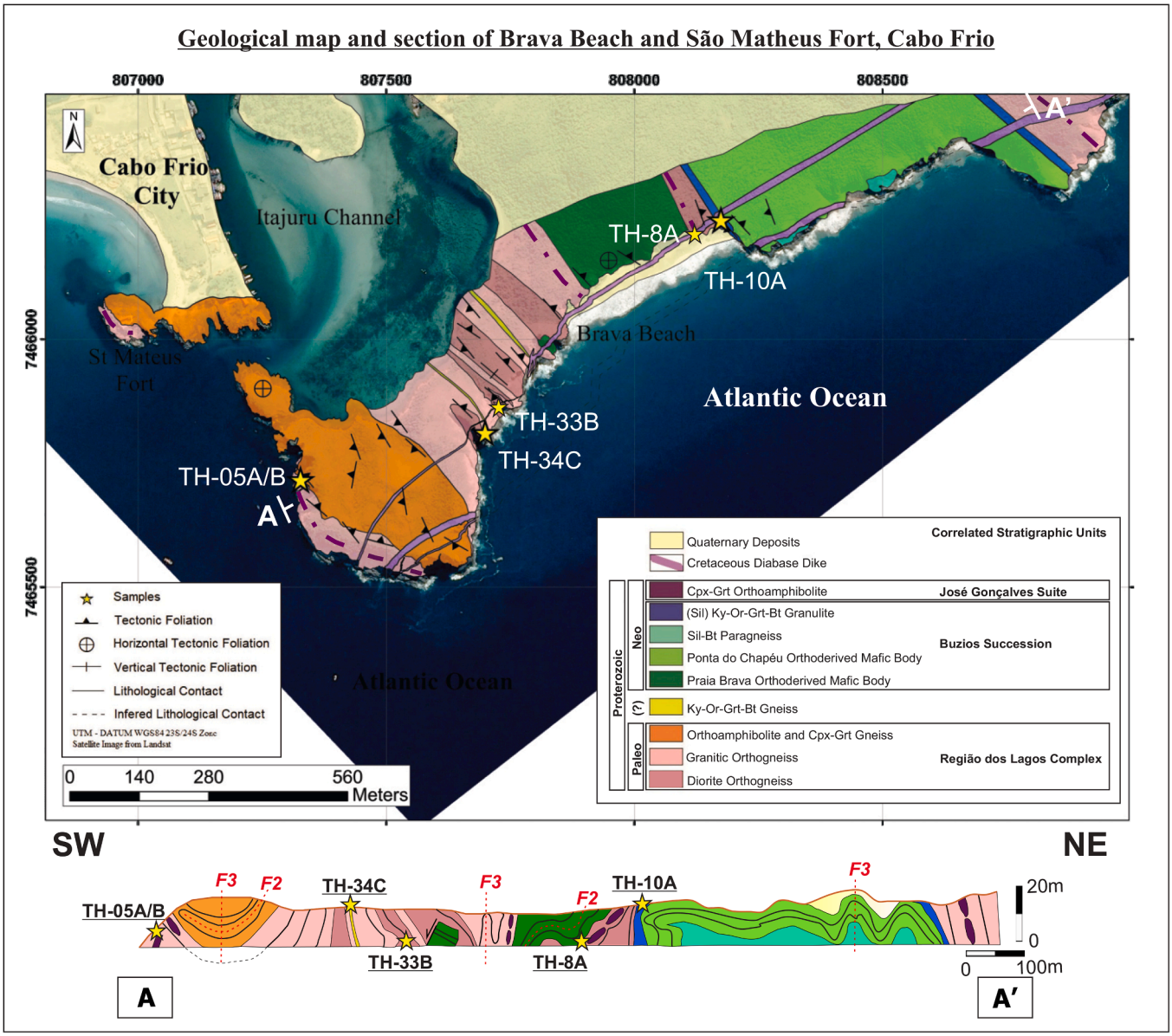

Fig. 2. (a) Geological map and (b) geological cross section of the Brava beach area in Cabo Frio. Samples analyzed in this paper are located on the map and on the section.

axial plane foliations indicating that melting was present at least during these two folding phases (Fig. 3e). Locally the contrasting rheology resulted in complex geometries (Figs. 2 and 3). However, the area is still considered suitable to test whether these two distinct rock associations shared the same *P-T*-t paths.

4.1.1. *Dioritic and granitic orthogneisses (Região dos Lagos Complex)*

Dioritic and granitic orthogneisses are correlated with the Região dos Lagos Complex, and referred here as the Paleoproterozoic basement, confirmed by U-Pb geochronological data (Vieira et al., unpublished results). These lithotypes contain leucosome veins locally, sub-parallel to parallel to the main foliation, defining a stromatic structure (Fig. 3g). These partial melt products have a granodioritic composition in the dioritic gneisses and a monzogranitic to alkali-feldspar granitic composition in the granitic gneisses. These orthogneisses, with diorites and granites as protoliths, predominate in the southwestern portion of the studied area (Fig. 2).

The dioritic orthogneiss crops out as layers of 50 m interleaved with the granitic orthogneiss (Fig. 2 and 3c). Two representative samples were analyzed in order to obtain temperature estimates from the pair hornblende-plagioclase (samples TH-8A and TH-33B). Samples are coarse-grained, with plagioclase (45%) and amphibole (42%), as

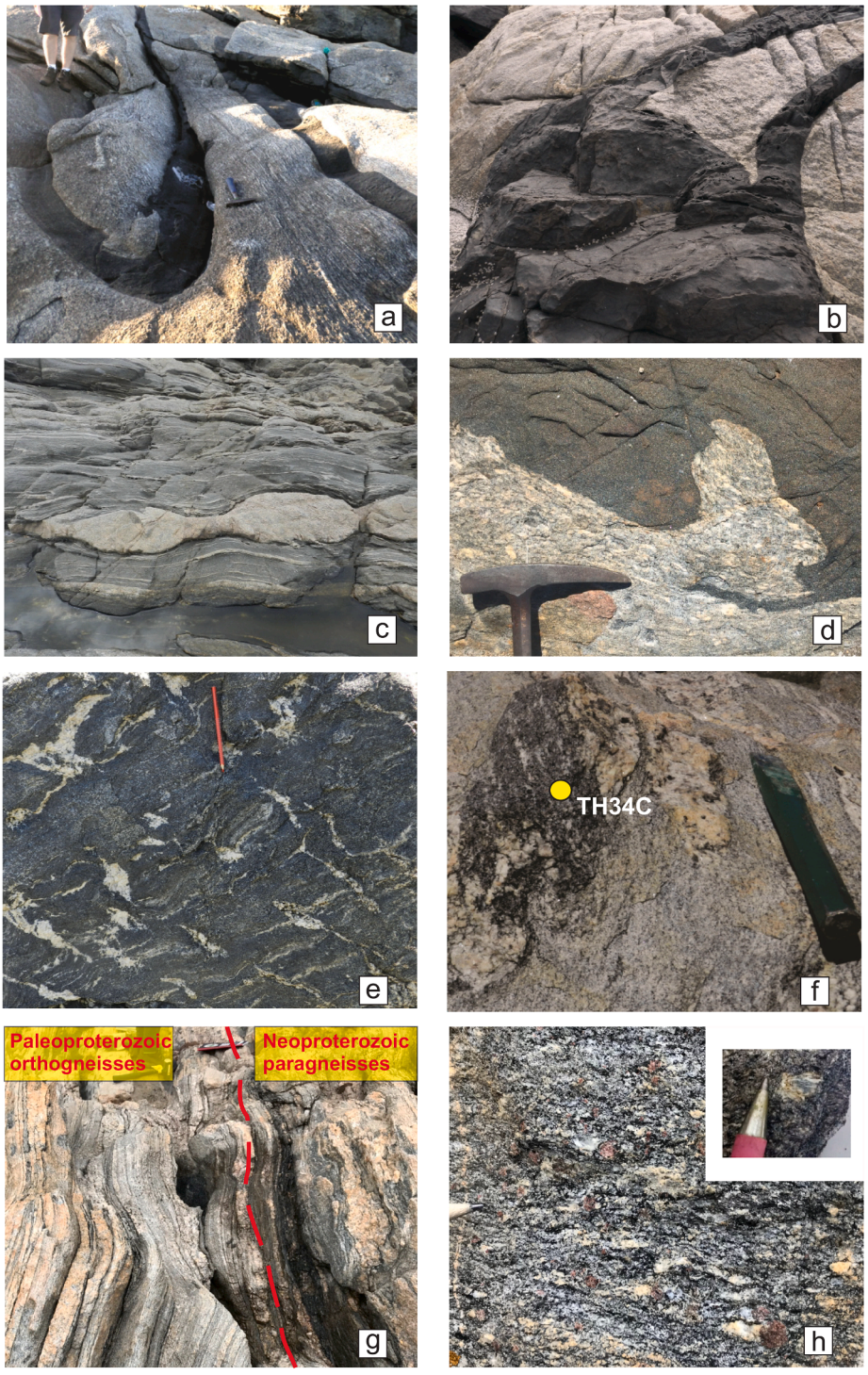

Fig. 3. (a) High strain domain in the Paleoproterozoic granitic orthogneisses with the amphibolite isoclinally folded. (b) Low strain domain with the garnet-clinopyroxene amphibolite (sample TH-5A) cross cutting the Paleoproterozoic granitic orthogneisses. (c) Paleoproterozoic orthogneisses with intercalation of dioritic and granitic compositions. (d) Sinuous contact between the granitic orthogneiss and garnet-clinopyroxene amphibolite related with the intrusion of the latter (detail in the paleodyke of Fig. 2b. (e) Ediacaran clinopyroxene amphibolite (Búzios Succession) with local partial melt and centimetric leucosome veins parallel to the axial plane of F3 folds. (f) kyanite-orthoclase-garnet-biotite gneiss layer (TH-34C) enclosed in the Paleoproterozoic granitic orthogneisses. (g) Tectonic contact between the Paleoproterozoic dioritic orthogneiss (Região dos Lagos Complex) and Ediacaran paragneisses (Búzios Succession) in a high strain zone with migmatites. (h) Ediacaran kyanite-orthoclase-garnet-biotite granulite with retrometamorphic sillimanite (TH-10A – Búzios Succession). Inset in upper right shows fibrolitic sillimanite overgrowing kyanite.

essential components, accessory biotite (5%), quartz (5%) and K-feldspar (3%), apatite, titanite, magnetite, ilmenite, sulfides, rutile and zircon as trace minerals. In thin section, granoblastic texture predominates.

The granitic orthogneiss preserves oriented euhedral to subhedral K-feldspar megacrysts in low strain domains (Fig. 3d). It is medium- to coarse-grained, equigranular to porphyritic, and contains plagioclase (An_{21-36}; 35–40%), quartz (20–25%), biotite (8–15%), hornblende (5–7%) and microcline (18–13%), the latter up to 5 cm long. Amphibole and biotite show rectilinear contacts, suggesting equilibrium; ilmenite often exhibits titanite rims. As observed in thin section, granoblastic texture predominates. Locally an isotropic fine-grained hololeucocratic metagranite crosscuts both units.

In addition, a paragneiss lens was mapped within the Paleoproterozoic orthogneisses, located in a high strain and migmatized domain (Fig. 3f), sample TH-34C). In the low strain and non-migmatized domains where original igneous structures are preserved (i.e., metadiorite enclaves in the metagranitoids), mafic paleodykes crosscut the metagranitoids (Fig. 3b, samples TH-5A and TH-5B).

4.1.2. *Kyanite-orthoclase-garnet-biotite gneiss (undetermined unit, sample TH-34C)*

A 1.5-meter-thick lens of kyanite-orthoclase-garnet-biotite gneiss, enclosed within the Paleoproterozoic orthogneisses, was selected for geothermobarometric and geochronological analyses (sample TH-34C – Fig. 2 and 3f). The widespread stromatic structure is parallel to the tectonic foliation of the granitic orthogneiss (Fig. 3f). The mineralogical composition is quartz (35%), biotite (20%), garnet (20%), perthitic orthoclase (15%) and kyanite (8%), with subordinate amounts of microcline and oligoclase (Fig. 4c and d). Rutile, apatite, zircon, monazite, and ilmenite are accessory minerals (Fig. 4d). Symplectitic plagioclase occurs between garnet and biotite. Myrmekite is observed where both feldspars are in contact. Garnet occurs as porphyroblasts (2 mm to 1 cm in diameter), usually with inclusions of biotite, quartz, plagioclase, zircon, monazite and opaque minerals (Fig. 4c and d). Kyanite appears as crystals up to 2 mm, in equilibrium with orthoclase and garnet (Fig. 4c and d). K-feldspar porphyroblasts reach up to 1 mm in size (Fig. 4c and d). Anhedral rutile crystals are included in biotite from the matrix.

4.1.3. *Garnet-clinopyroxene amphibolite (José Gonçalves Suite, sample TH-5A and TH-5B)*

Mafic bodies of garnet-clinopyroxene amphibolite, 5 cm up to 5 m thick, cross cut the Paleoproterozoic orthogneisses (Fig. 2, 3a and 3b). These paleodykes are correlated to the José Gonçalves Suite. Even with the metamorphic overprint, some mafic bodies preserve their original

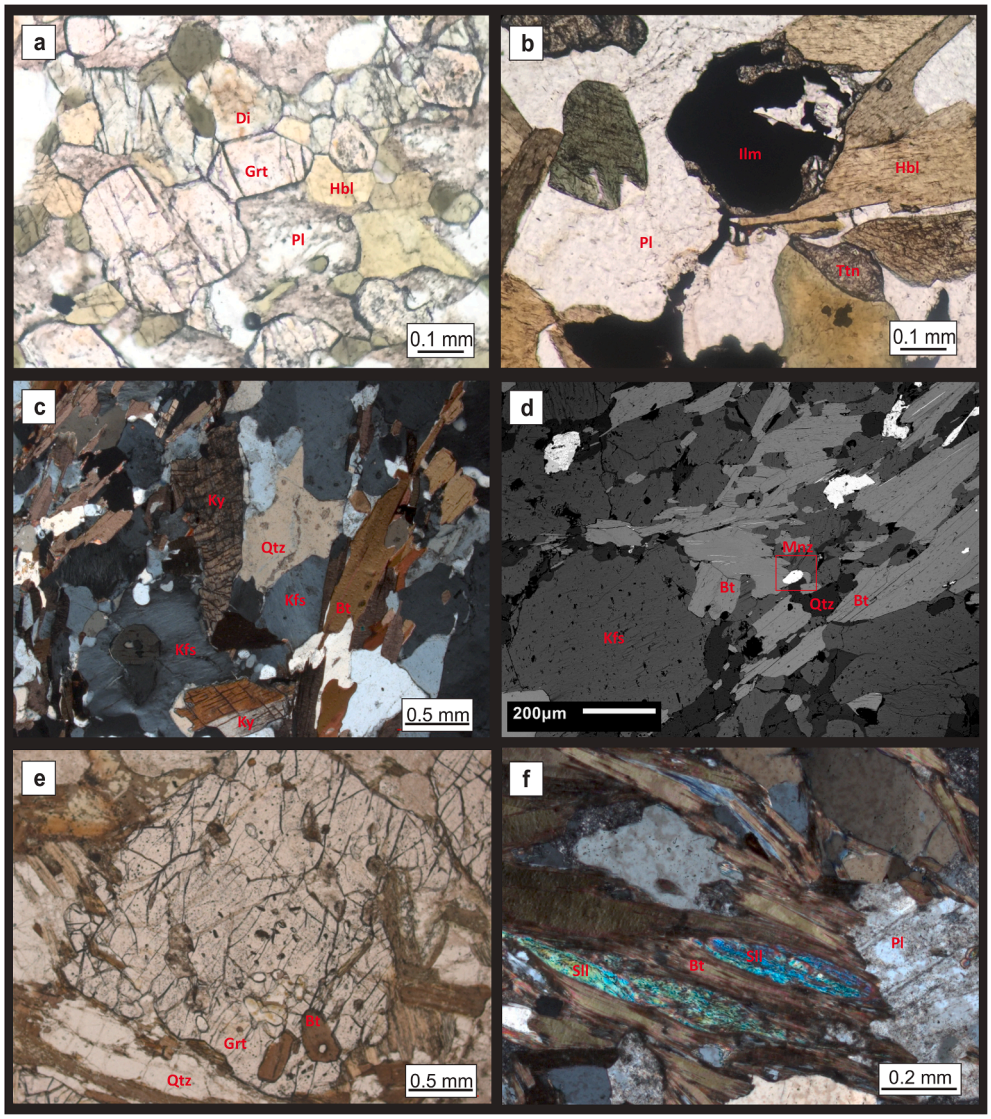

Fig. 4. (a) Fine grained garnet-clinopyroxene amphibolite cutting the Paleoproterozoic orthogneiss, with granoblastic texture and mineral equilibrium between diopside-garnet-hornblende (sample TH-5A – José Gonçalves Suite). (b) Ilmenite with titanite rim in the fine-grained garnet-clinopyroxene amphibolite (sample TH-5A); (c) Kyanite-orthoclase in equilibrium inside the kyanite-orthoclase-garnet-biotite gneiss (sample TH-34C); (d) Back-scattered electron (BSE) image of sample TH-34C sample showing monazite crystals in the matrix. (e) Garnet porphyroblast with inclusions of biotite, quartz, feldspar, zircon, monazite and opaque minerals (sample TH-10A – Búzios Succession). (f) Fibrolitic sillimanite intergrown with biotite (sample TH-10A). Abbreviations according to Kretz (1983).

igneous grain size variation (fine-grained at the border, coarse-grained at the center). Contacts are usually sharp (Fig. 3b), straight to locally sinuous (Fig. 3d). In high strain domains, the metabasites show isoclinal folds (Fig. 3a) and boudins parallel to the orthogneiss foliation. Locally they display partial melt features with leucosome, mostly composed of plagioclase and quartz (Fig. 3e). The garnet-clinopyroxene amphibolite has hornblende (34–60%), plagioclase (25–39%), diopside (10–23%) and garnet (8–18%) as essential minerals, and quartz (1–2%), titanite (2–5%), biotite (2–5%) ilmenite (2%), magnetite (1%), rutile (trace), apatite (trace) and zircon (trace) as accessory minerals. In thin section the granoblastic texture is dominant (Fig. 4a).

Two samples from a fine-grained homogeneous garnet-clinopyroxene amphibolite body were selected for geothermobarometric studies (TH-5A and 5B– Fig. 2 and 3b, 3d). They were sampled in a low strain domain, without evidence of partial melting, and has a granoblastic texture in thin section. Diopside coexists in equilibrium with pargasite (Fig. 4a) and both minerals are partially replaced by actinolite. The anorthite content in plagioclase varies from An_2 (rim) to An_{49} (core). Titanite is surrounding ilmenite (Fig. 4b). Three different metamorphic assemblages were identified: 1. diopside + garnet + andesine (An_{49}) + quartz + pargasite + rutile + ilmenite (granulite-amphibolite facies, Fig. 4a); 2. hornblende + andesine + titanite (amphibolite facies); 3. albite + actinolite + biotite + chlorite + sericite + epidote (greenschist facies).

4.1.4. Kyanite-orthoclase-garnet-biotite granulite with retrometamorphic sillimanite (Búzios Succession, sample TH-10A)

In the northeastern part of the area, the Paleoproterozoic orthogneisses are in contact with Ediacaran paragneisses and associated banded amphibolite bodies (Fig. 2), which are correlated to the Búzios Succession, part of the Neoproterozoic supracrustals of the Cabo Frio Tectonic Domain, confirmed by U-Pb geochronological data from Capistrano et al. (2020, Fig. 2). The contact with the dioritic orthogneiss is a subvertical NW-SE high strain zone with strike-slip stretching lineation and widespread migmatization (Fig. 3g). Despite the deformation and metamorphism, the compositional banding reflects, at least in part, a primary bedding related to sedimentary and volcanic protoliths. Two groups of mafic bodies are described: (1) laminated and massive amphibolitic gneisses, >50 m thick with minor garnet amphibolite, diopside amphibolite and hornblende residue association; (2) centimetric to metric amphibolite layers interleaved with aluminous gneiss and calc-silicate rocks (Schmitt et al., 2008; Capistrano et al., 2020).

We selected a 2 m thick layer of kyanite-orthoclase-garnet-biotite granulite with retrometamorphic sillimanite layer to represent the Búzios Succession in our *P-T*-t studies (Sample TH-10A, Fig. 2 and 3h). It is intercalated with fine-grained amphibolite, quartzite and calc-silicate rock layers (Fig. 2). The layer is folded, but structurally concordant with the Paleoproterozoic dioritic orthogneiss (Fig. 2 and 3g). The selected sample from the melt-poor part of the migmatite, contains quartz (30%), biotite (20%), garnet (20%), orthoclase (16%) and kyanite (10%), a lower proportion of microcline and plagioclase (oligoclase-andesine). Titanite, rutile, apatite, zircon, monazite, tourmaline and ilmenite are accessory minerals. Kyanite occurs as individual crystals up to 2 cm in textural equilibrium with orthoclase, plagioclase and garnet. Garnet occurs as porphyroblasts up to 1 cm in diameter, usually with inclusions of biotite, quartz, feldspar, zircon, monazite and opaque minerals (Fig. 4e). Sillimanite partially replaces kyanite, forming pseudomorphs (Fig. 3h) and locally developing fibrolite intergrowth with biotite (Fig. 4f). The inclusion trails define an internal foliation in the garnet. The symplectite is localized along the contact between biotite and garnet, together with a lamellar and vermicular fine-grained intergrowth of plagioclase. Porphyroblasts of K-feldspar form crystals of up to 1 cm in length. Plagioclase shows myrmekite and antiperthite and is locally replaced by sericite and carbonate. Chlorite partially replaces biotite and muscovite replaces in part biotite and K-feldspar. The selected sample has similar composition to the aluminous gneiss layer within the basement unit (Sample TH-34C – Fig. 3h), and is therefore suitable for *P-T* data comparison.

4.2. Mineral chemistry

4.2.1. Diorite orthogneiss (Região dos Lagos Complex, TH-8A and TH-33B)

The amphibole has a composition varying from magnesio-hornblende to pargasite (Fig. 5d). In general, the amphibole from sample TH-33B has X_{Mg}, Ti and Al content ranging, respectively, from 0.42 to 0.44, 0.13 to 0.16 apfu and 1.71 to 1.89 apfu. For the amphibole from sample TH-8A, X_{Mg}, Ti and Al content vary, respectively, from 0.46 to 0.49, 0.10 to 0.16 apfu and 1.50 to 1.69 apfu. TH-33B contains oligoclase with average composition of An_{26-28}, and in sample TH-8A plagioclase composition is An_{32-33} (Fig. 5c).

4.2.2. Kyanite-orthoclase-garnet-biotite gneiss (nameless unit, sample TH-34C)

The garnet composition is dominated by the almandine (78 to 82%), followed by pyrope (12 to 16%), grossular (3 to 4%) and spessartine end-member (2 to 3%). The compositional profiles are almost flat, with slight increase of Fe and decrease of Mg towards the rims (Fig. 5a). Orthoclase has no compositional variation and contains between 5 and 6% of albite molecule with pure albite exsolution lamellae (perthitic texture). The compositional variation of plagioclase ranges from An_3 to An_{16}, respectively in rims and cores (Fig. 5c). The biotite composition is homogeneous with no significant variation from core to rim and X_{Mg} between 0.49 and 0.57 (Fig. 5e). The Ti content is high, with values varying from 0.22 to 0.29 apfu.

4.2.3. Garnet-clinopyroxene amphibolite (José Gonçalves Suite, samples TH-5A and TH-5B)

The garnet composition is controlled by end-members almandine, with values between 57 and 61%, grossular varying from 19 to 22%, pyrope, 15 to 18% and spessartine, 2 to 4% (Fig. 5a). Although the garnet grains have considerable chemical variation in the rock, the one from Fig. 5a has a flat profile, with almandine $_{59-61}$, grossular $_{20-21}$ pyrope $_{15-18}$, spessartine $_{2-3}$. There is a slight increase in the almandine from core to rim, while pyrope and grossular contents decrease. Low spessartine contents vary between 2 and 4% (Fig. 5a). Significant compositional variations in plagioclase, from core to rim, occur in both samples (Fig. 5c). All rims are almost pure albite (An_{1-10}), whilst the cores are andesine (An_{40-50}). The clinopyroxene is diopside (Fig. 5b) and the core and rims of the crystals have practically no chemical variation, with X_{Mg} varying between 0.58 and 0.66, and aluminum ranging from 0.02 to 0.16 apfu. The pargasite has cores with higher in Al (2.1 apfu) when compared with the rim (1.7 apfu). In general, the Ti content is 0.2 apfu and X_{Mg} ranges from 0.45 to 0.49 (Fig. 5d).

4.2.4. Kyanite-orthoclase-garnet-biotite granulite with retrometamorphic sillimanite (Búzios Succession, sample TH-10A)

The garnet crystals from sample TH-10A have composition controlled by almandine end-members, significant grossular and pyrope components, with an evident core to rim variation (Fig. 5a). These crystals have a core relatively rich in grossular and pyrope, with 20–25% and 18–25% respectively, and comparatively poor in almandine, with 52–56%, while the rims have 62–70% of almandine, 4–9% of grossular and 28–30% of pyrope (Fig. 5a). The plagioclase has compositional zoning, with composition An_{45} in the core and An_{23} in the rim (Fig. 5c). Orthoclase is perthitic with pure albite as exsolution. The biotite grains have Ti contents ranging from 0.01 to 0.05 apfu and X_{Mg} between 0.60 and 0.67 (Fig. 5e).

4.3. Thermobarometry

The hornblende-plagioclase thermometer (Holland and Blundy,

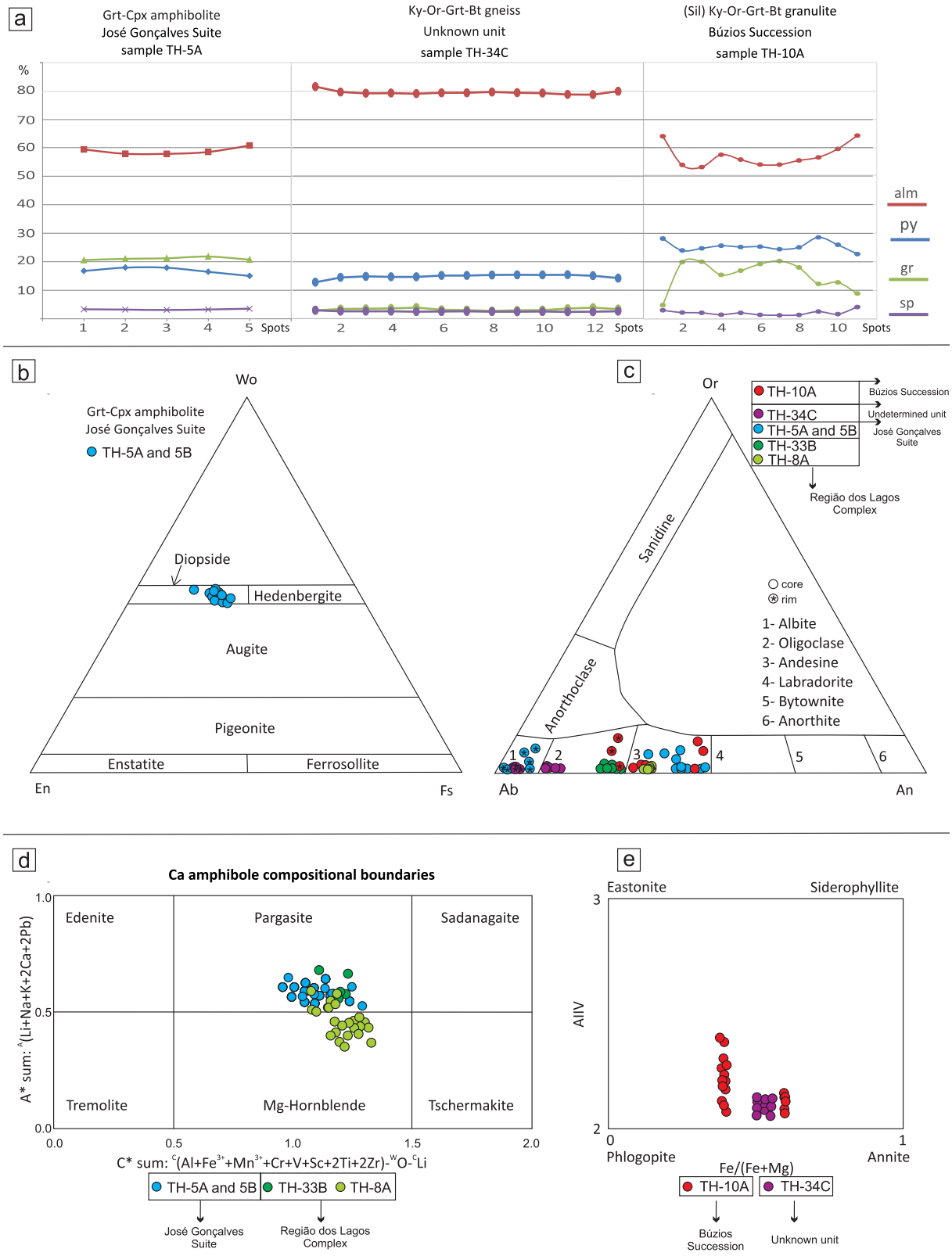

Fig. 5. Mineral chemistry of Região dos Lagos Complex (dioritic orthogneiss, samples TH-8A and TH-33B), José Gonçalves Suite (garnet-clinopyroxene amphibolite, samples TH-5A and TH-5B), undetermined unit (kyanite- orthoclase-garnet-biotite gneiss, sample TH-34C) and Búzios Succession (kyanite-orthoclase-garnet-biotite granulite with retrometamorphic sillimanite, sample TH-10A). (a) Representative garnet zoning profiles for the three samples. (b) Chemical composition of pyroxene from garnet-clinopyroxene amphibolite (samples TH-5A and TH-5B). (c) Chemical composition of plagioclase from all samples. (d) Chemical composition of amphibole from garnet-clinopyroxene amphibolite and diorite orthogneiss (samples TH-5A, TH-5B, TH-8A and TH-33B). (e) Chemical composition of biotite from both paragneisses (samples TH-34C and TH- 10A).

1994), based on the number of Si- and Al-cations in the tetrahedron positions of amphibole, was applied to two dioritic orthogneiss samples (Região dos Lagos Complex). The results yielded temperatures between 759 °C (sample TH-8A) and 772 °C (sample TH-33B), calculated for a pressure of 10 kbar.

Pressure and temperature determinations, using THERMOCALC, v.3.32, average *P-T* mode (Powell and Holland 1994) were performed on 4 samples (TH-5A, TH-5B, TH-34C and TH-10A). The temperature and pressure are calculated separately, then the two variables were calculated together with the average *P-T* method (Powell and Holland 1994).

The kyanite-orthoclase-garnet-biotite gneiss enclosed within Paleoproterozoic granitic orthogneiss (sample TH-34C) yields pressure and temperature conditions of 10.1 ± 0.5 kbar and 818 ± 70 °C (Fig. 6b and Table 2). This represents the metamorphic near peak, with the core compositions of the minerals garnet, K-feldspar, plagioclase, biotite in paragenesis with kyanite, quartz and excess H_2O.

Samples TH-5A and TH-5B (garnet-clinopyroxene amphibolite – José Gonçalves Suite) show *P-T* conditions respectively of 9.7 ± 0.7 kbar and 825, ± 35 °C and 10.1 ± 1.1 kbar and 825 ± 46 °C, based on mineral core compositions of garnet, clinopyroxene, hornblende and plagioclase, in the presence of quartz (Fig. 6a and Table 2). For sample TH-5B, *T* and *P* were calculated separately; for sample TH-5A, the calculation was simultaneous, using the average *P-T* mode. It appears that both rocks which are either included or that cross cutting the Paleoproterozoic orthogneisses, the kyanite-orthoclase-garnet-biotite gneiss (TH-34C) and the garnet-clinopyroxene amphibolite (TH-5A and 5B) yielded similar *P-T* results.

For the Ediacaran kyanite-orthoclase-garnet-biotite granulite with retrometamorphic sillimanite (sample TH-10A Búzios Succession), *P-T* conditions of 15.0 ± 0.6 kbar and 817 ± 24 °C were calculated simultaneously, using the average *P-T* mode (Fig. 6b and Table 2). Calculations for the metamorphic near-peak mineral assemblage considered mineral core compositions from garnet, K-feldspar, plagioclase, and biotite in the presence of kyanite and quartz with H_2O in excess. There is not much difference in the results when pressure and temperature are calculated separately, giving values of 14.2 ± 0.4 kbar and 790 ± 18 °C. For the retrograde stage, calculations considered mineral rim compositions of garnet, K-feldspar, plagioclase and biotite in the presence of sillimanite and quartz with H_2O in excess. The conditions calculated on average *P-T* mode for the retrograde mineral assemblage are 10.8 ± 0.7 kbar and 800 ± 27 °C. When calculated separately, *P-T* conditions are 9.5 ± 1.1 kbar and 796 ± 23 °C (Fig. 6b and Table 2).

4.4. Zr-in-rutile

In the two paragneiss samples, kyanite-orthoclase-garnet-biotite gneiss (TH-34C) and kyanite-orthoclase-garnet-biotite granulite with retrometamorphic sillimanite (TH-10A, Búzios Succession), the Zr-in-rutile technique was used as a geothermometer, combined with pressures calculated previously by THERMOCALC, 10 kbar and 15 kbar respectively (Figs. 6, 7 and Supplementary Table 3).

In sample TH-34C, from the paragneiss lens enclosed within Paleoproterozoic orthogneisses, the Zr content varies from 893 to 441 ppm and the calculated temperature varies between 747 ± 4 °C and 682 ± 6 °C (Supplementary Table 3 and Figs. 6 and 7). In sample TH-10A from the Búzios Succession, the rutile crystals included in garnet porphyroblasts show Zr concentration between 1012 ppm and 282 ppm, with calculated temperature ranging from 783 ± 3 °C to 666 ± 9 °C (Supplementary Table 3 and Figs. 6 and 7).

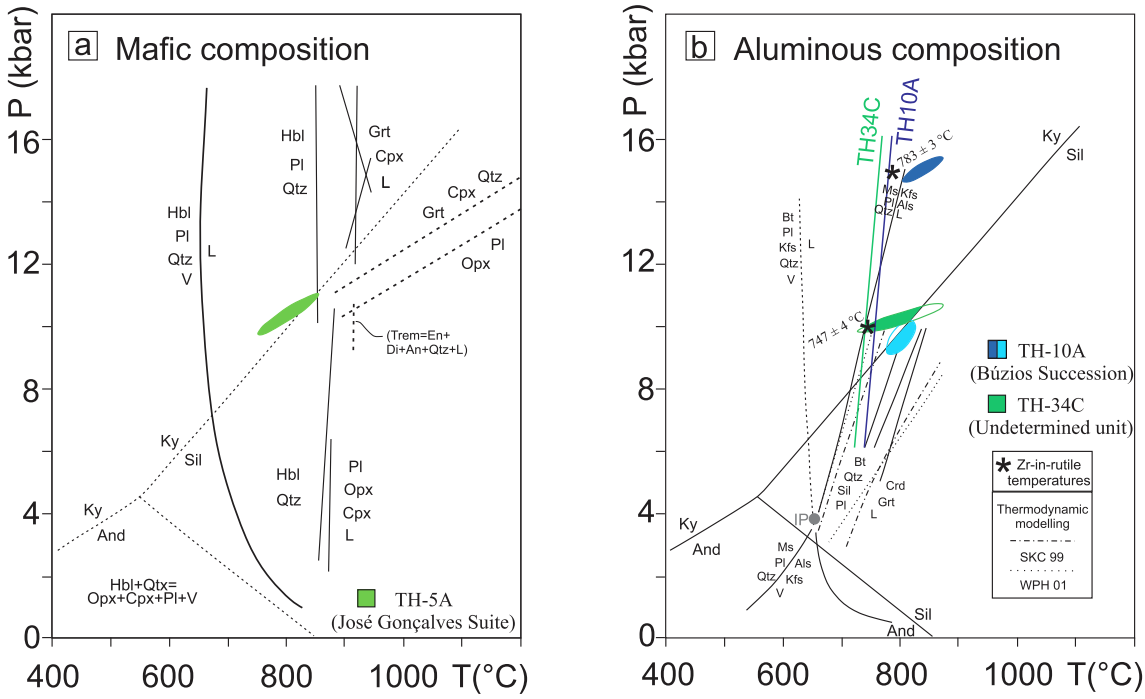

Fig. 6. *P-T* conditions calculated with THERMOCALC for three samples. (a) garnet-clinopyroxene amphibolite from sample TH-5A (light green ellipse) plotted in a petrogenetic grid for mafic rocks, with a compilation of reactions by Pattison et al. (2003). (b) kyanite-orthoclase-garnet-biotite gneiss from undetermined unit (TH-34C – dark green ellipse) and kyanite-orthoclase-garnet-biotite granulite with retrometamorphic sillimanite from the Búzios Succession (TH-10A – blue ellipses), both plotted on grids for aluminous composition, with compilation of reactions by Pattison et al. (2003). For the last sample, the dark and light blue ellipses represent respectively *P-T* conditions for near-peak and decompression. The green and blue lines, for samples TH-34C and TH-10A respectively, are Zr in rutile isopleths according to Tomkins et al. 2007. These lines represent the temperature range for pressures ranging from 6 to 16 kbar. *747 ± 4 °C is the minimum metamorphic temperature for the kyanite-orthoclase-garnet-biotite gneiss from the undetermined unit (sample TH-34C); and it is provided by Zr-in-rutile technique at 10 kbar. *783 ± 3 °C is the minimum metamorphic temperature for the kyanite-orthoclase-garnet-biotite granulite with retrometamorphic sillimanite from the Búzios Succession (sample TH-10A); it is provided by Zr-in-rutile technique at 15 kbar. IP is an invariant point. Spear et al. (1999, SKC 99). White et al. (2001, WPH 01).

Table 2
Mineral composition data used in geotermobarometric calculations by THERMOCALC.

Sample	TH-5A				TH-5B			
Mineral	Grt (core)	Cpx (core)	Pl (core)	Hbl (core)	Grt (core)	Cpx (core)	Pl (core)	Hbl (core)
SiO_2	38.11	50.27	59.61	42.49	38.49	51.27	57.59	42.95
TiO_2	0.00	0.00	0.00	1.64	0.00	0.00	0.00	1.52
Al_2O_3	21.35	4.45	25.85	11.14	20.82	2.53	26.45	10.99
Cr_2O_3	0.01	0.02	0.00	0.00	0.02	0.00	0.00	0.00
Fe_2O_3	0.00	1.71	0.00	1.8	0.00	2.39	0.00	2.55
FeO	26.31	9.2	0.00	18.47	27.51	8.37	0.00	16.15
MnO	1.14	0.28	0.00	0.14	1.59	0.36	0.00	0.12
MgO	4.73	11.12	0.00	9.94	3.85	11.94	0.00	9.72
CaO	7.52	22.29	8.14	11.41	7.38	22.73	8.71	11.80
Na_2O	0.00	0.49	6.70	2.14	0.00	0.47	6.56	2.04
K_2O	0.00	0.00	0.09	0.32	0.00	0.00	0.05	0.38
Totals	99.17	99.84	100.39	99.79	99.65	100.06	99.36	98.69
Oxygens	12	6	8	0.23	12	6	8	23
Si	3.01	1.89	2.64	6.33	3.04	1.93	2.59	6.44
Ti	0.00	0.00	0.00	0.18	0.00	0.00	0.00	0.17
Al	1.99	0.2	1.35	1.96	1.94	0.11	1.4	1.94
Cr	0.00	0.00	0.00	0.00	0.00	0.00	0.00	0.00
Fe3	0.00	0.05	0.00	0.2	0.00	0.07	0.00	0.29
Fe2	1.74	0.29	0.00	2.3	1.82	0.26	0.00	2.02
Mn	0.08	0.01	0.00	0.02	0.11	0.01	0.00	0.02
Mg	0.56	0.62	0.00	2.21	0.45	0.67	0.00	2.17
Ca	0.64	0.9	0.39	1.87	0.63	0.92	0.42	1.90
Na	0.00	0.04	0.58	0.62	0.00	0.03	0.57	0.59
K	0.00	0.00	0.01	0.06	0.00	0.00	0.00	0.07
Sum	8	4	5	16	8	4		16
End-member	Alm 58% Prp 18% Grs 21% Sps 3%	$X_{Mg} = 64$	An_{39}	$X_{Mg} = 47$	Alm 61% Prp 15% Grs 21% Sps 4%	$X_{Mg} = 66$	An_{42}	$X_{Mg} = 48$

Sample	**TH-34C**			
Mineral	**Grt (core)**	**Bt (core)**	**Pl (core)**	**Kfs (core)**
SiO_2	37.85	34.76	65.48	65.01
TiO_2	0.00	4.27	0.00	0.00
Al_2O_3	20.39	21.39	21.36	19.60
Cr_2O_3	0.00	0.00	0.00	0.00
Fe_2O_3	1.99	1.85	0.01	0.08
FeO	31.98	15.46	0.00	0.00
MnO	1.10	0.00	0.00	0.00
MgO	5.91	10.50	0.00	0.00
CaO	1.27	0.00	2.40	0.11
Na_2O	0.00	0.00	10.45	2.96
K_2O	0.00	6.39	0.11	11.87
Totals	100.49	94.63	99.81	99.63
Oxygens	12	11	8	8
Si	2.99	2.57	2.89	2.97
Ti	0.00	0.24	0.00	0.00
Al	1.90	1.87	1.11	1.05
Cr	0.00	0.00	0.00	0.00
Fe3	0.12	0.10	0.00	0.00
Fe2	2.11	0.96	0.00	0.00
Mn	0.07	0.00	0.00	0.00
Mg	0.70	1.16	0.00	0.00
Ca	0.11	0.00	0.11	0.01
Na	0.00	0.00	0.89	0.26
K	0.00	0.60	0.01	0.69
Sum	8	8	5	5
End-member	Alm 72% Prp 22% Grs 3% Sps 2%	$X_{Mg} = 52$	An_{11}	

Sample	**TH-33B**		**TH-8A**	
Mineral	**Hbl**	**Pl**	**Hbl**	**Pl**
SiO_2	40.84	61.73	42.30	59.89
TiO_2	1.43	0.00	1.07	0.00
Al_2O_3	11.75	24.74	11.10	24.43
Cr_2O_3	0.00	0.00	0.00	0.00
Fe_2O_3	4.33	0.15	4.91	0.15
FeO	17.02	0.00	14.03	0.00
MnO	0.04	0.00	0.36	0.00
MgO	8.42	0.00	9.34	0.00

(*continued on next page*)

Table 2 (*continued*)

Sample	TH-33B		TH-8A	
Mineral	Hbl	Pl	Hbl	Pl
CaO	11.74	5.29	11.65	6.90
Na_2O	1.59	7.86	1.26	7.58
K_2O	1.52	0.26	0.43	0.11
Totals	98.68	100.04	96.45	99.06
Oxygens	23	8	23	8
Si	6.20	2.73	6	2.69
Ti	0.16	0.00	0.122	0.00
Al	2.11	1.29	1.989	1.30
Cr	0.00	0.00	0.000	0.00
Fe3	0.50	0.01	0.562	0.01
Fe2	2.16	0.00	1.783	0.00
Mn	0.01	0.00	0.046	0.00
Mg	1.91	0.00	2.115	0.00
Ca	1.91	0.25	1.898	0.33
Na	0.47	0.67	0.370	0.66
K	0.29	0.02	0.083	0.01
Sum	16	5	16	5
	$X_{Mg} = 42\%$	An_{25}	$X_{Mg} = 47\%$	An_{33}

Sample	TH-10A							
Mineral	Grt (core)	Grt (rim)	Bt (core)	Bt (rim)	Pl (core)	Pl (rim)	Kfs (core)	Kfs (rim)
SiO_2	38.95	38.15	37.26	36.49	60.74	60.95	65.98	66
TiO_2	0.00	0.00	2.45	2.58	0.00	0.00	0.00	0.00
Al_2O_3	21.65	21.44	17.21	16.87	25.16	25.23	19.26	19.1
Cr_2O_3	0.00	0.01	0.00	0.00	0.00	0.00	0.00	0.00
Fe_2O_3	0.00	0.00	0.00	0.00	0.03	0	0.07	0.00
FeO	24.73	28.64	13.26	15.63	0.00	0.00	0.00	0.00
MnO	0.60	1.85	0.00	0.00	0.00	0.00	0.00	0.00
MgO	6.27	5.70	15.02	13.59	0.00	0.00	0.00	0.00
CaO	7.25	3.11	0.00	0.00	7.01	6.87	0.03	0.02
Na_2O	0.00	0.00	0.00	0.00	7.56	7.7	0.14	0.12
K_2O	0.00	0.00	9.59	9.87	0.10	0.1	15.13	14.61
Totals	99.45	98.90	94.79	95.03	100.60	100.85	100.61	99.85
Oxygens	12	12	11	11	8	8	8	8
Si	3.03	3.02	2.77	2.74	2.69	2.69	3.00	3.01
Ti	0.00	0.00	0.14	0.15	0.00	0.00	0.00	0.00
Al	1.98	2.00	1.51	1.50	1.31	1.31	1.03	1.03
Cr	0.00	0.00	0.00	0.00	0.00	0.00	0.00	0.00
Fe3	0.00	0.00	0.00	0.00	0.00	0.00	0.00	0.01
Fe2	1.61	1.90	0.82	0.98	0.00	0.00	0.00	0.00
Mn	0.04	0.12	0.00	0.00	0.00	0.00	0.00	0.00
Mg	0.73	0.67	1.66	1.52	0.00	0.00	0.00	0.00
Ca	0.60	0.26	0.00	0.00	0.33	0.33	0.00	0.00
Na	0.00	0.00	0.00	0.00	0.65	0.66	0.01	0.01
K	0.00	0.00	0.91	0.95	0.01	0.01	0.88	0.85
Sum	8	8	8	8	5	5	5	5
End-member	Alm 54% Prp 25% Grs 20% Sps 1%	Alm 64% Prp 23% Grs 9% Sps 4%	$X_{Mg} = 67\%$	$X_{Mg} = 61\%$	An_{33}	An_{33}		

4.5. U-Pb in zircon

In order to constrain the crystallization and metamorphic age of the garnet-clinopyroxene amphibolite (sample TH-5A – José Gonçalves Suite; Fig. 3b), as well as the metamorphic and maximum depositional ages for the protolith of the kyanite-orthoclase-garnet-biotite gneiss (sample TH-34C – undetermined unit; Fig. 3f), U-Pb analyses on zircon were performed on both samples. The latter is included and the former cross cuts the Paleoproterozoic orthogneisses.

4.5.1. Kyanite-orthoclase-garnet-biotite gneiss (undetermined unit, sample TH-34C)

From the 188 zircon crystals, analyzed with U-Pb by LA-ICPMS, 170 were 90–110% concordant (Fig. 8a). In general, crystals are translucent to pink, subhedral–euhedral rounded or prismatic, with dimensions between 78 μm to 434 μm (Fig. 8d and 8e). Most cores show concentric oscillatory zoning with high Th/U ratios (0.19–3.45), indicating an igneous origin (Fig. 8d and 8e). Considering that this is an aluminous-paragneiss, these zircon domains were interpreted as representing the ages of the sedimentary sources, hence detrital zircon grains. The crystal rims are bright in CL-images and present low Th/U ratios (0.01 to 0.04), consistent with a metamorphic origin (Fig. 8c).

Probability density plots (PDP) were created using $^{206}Pb/^{238}U$ age for grains younger than 1.3 Ga and $^{207}Pb/^{206}Pb$ ages for grains older than 1.3 Ga. The results show a major detrital zircon population with $^{207}Pb/^{206}Pb$ ages ranging from 2.0 to 1.68 Ga (Fig. 8b), with a prominent peak at 1.95 Ga (Orosirian-Paleoproterozoic). This peak coincides with the same age of the protolith of the Paleoproterozoic orthogneisses (Região dos Lagos Complex) in which this paragneiss lens is enclosed. Two other minor peaks show Statherian sources of ca. 1.82 Ga and 1.72 Ga (Fig. 8b). The youngest detrital zircon has an age of ca. 1.68 Ga, interpreted here as the maximum depositional age for the protolith of sample TH-34C (see discussion).

Although the metamorphic rims were too thin to be analyzed with LA-ICPMS, three spots yielded concordant ages in the range between 546 and 529 Ma, with Th/U ratios below 0.03 (Fig. 8c). A concordia mean age of 533.8 ± 8 Ma was calculated, coherent with the Cambrian metamorphic event (see discussion – Fig. 8c). Spot #43.2 (593 ± 42 Ma)

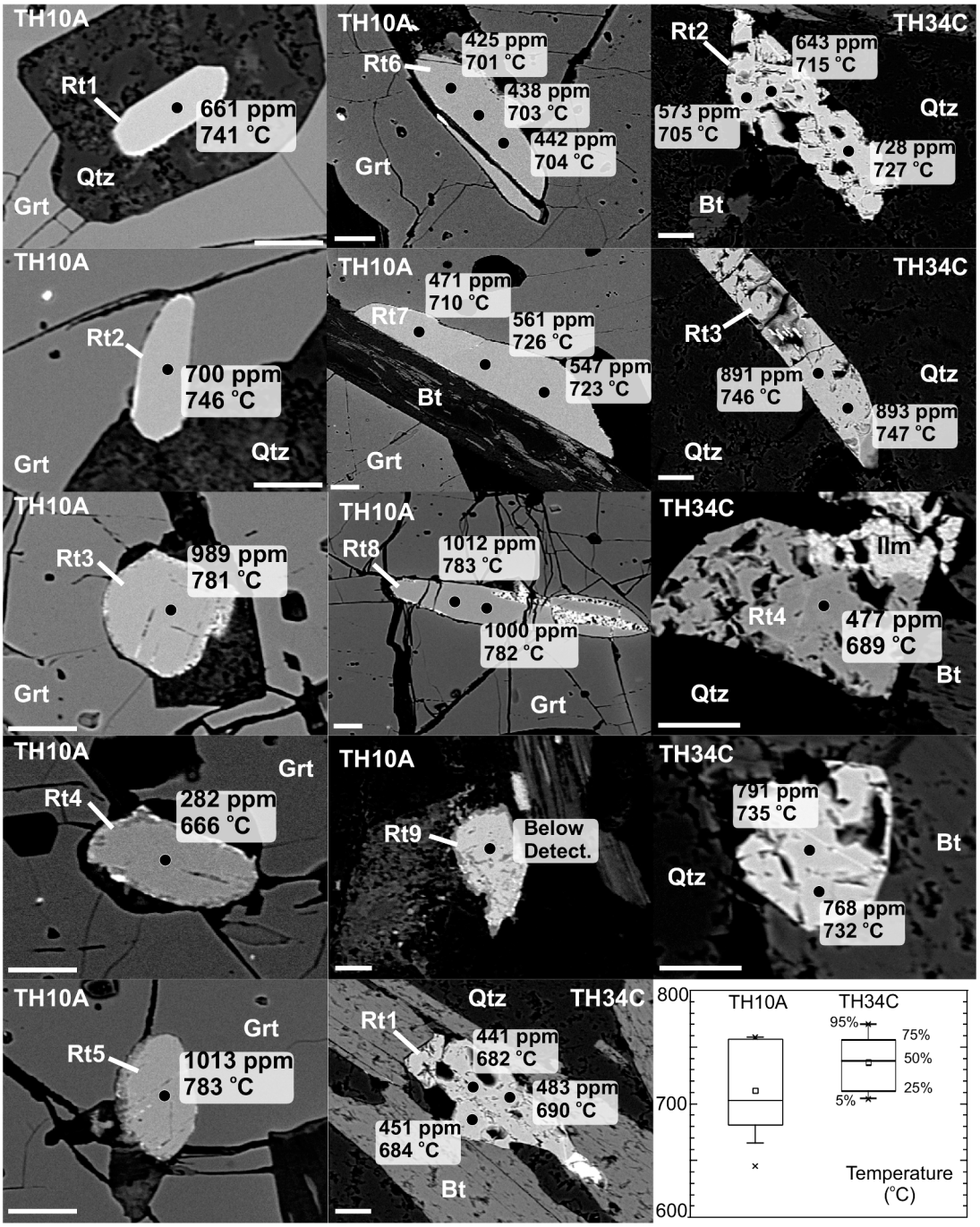

Fig. 7. Back-scattered electron (BSE) images of representative rutile grains with concentrations of Zr (in ppm). Boxplots showing concentration (in ppm) of Zr in rutile crystals from studied samples. Vertical lines show the 5th and 95th percentiles. Boxes represent the second (bottom-25%) and third quartile (top-75%). The square and horizontal line inside the boxes represent the average and the media, respectively. Only analyses above the minimum detection limit are presented. Analyzed samples are indicated on the top of each image, and correspond to kyanite bearing paragneisses (TH-34C, undetermined unit and TH-10A, Búzios Succession).

was excluded from the concordia age calculation, because it might represent a mixed age, due to the very thin metamorphic rim; part of the crystal core might also have been analyzed. (Fig. 8c).

4.5.2. Garnet-clinopyroxene amphibolite (José Gonçalves Suite, sample TH-5A)

The garnet-clinopyroxene amphibolite yielded few zircon crystals. In general, the crystals are translucent to pink, subhedral, rounded or prismatic, with dimensions between 190 μm to 230 μm (Fig. 9). Five grains were selected and 11 analyses were performed using U-Pb SHRIMP-II (Fig. 8 and Supplementary Table 2). $^{206}Pb/^{238}U$ measurements were considered for grains younger than 1.3 Ga and $^{207}Pb/^{206}Pb$ measurements, for grains older than 1.3 Ga.

The bright white to light gray number 1 crystal exhibits concentric oscillatory zoning with high Th/U ratios (0.86 to 1.16), indicating an igneous origin (Fig. 9a). Three spots yielded ages of ca. 1.95 Ga, 1.91 Ga and 1.84 Ga, consistent with the age of the country rock (Paleoproterozoic orthogneisses from the Região dos Lagos Complex- see discussion).

Grain 6 has clear igneous oscillatory zoning in its core, with ages of 561 ± 6 Ma and 573 ± 5 Ma (Fig. 9a). This domain shows also high Th/U

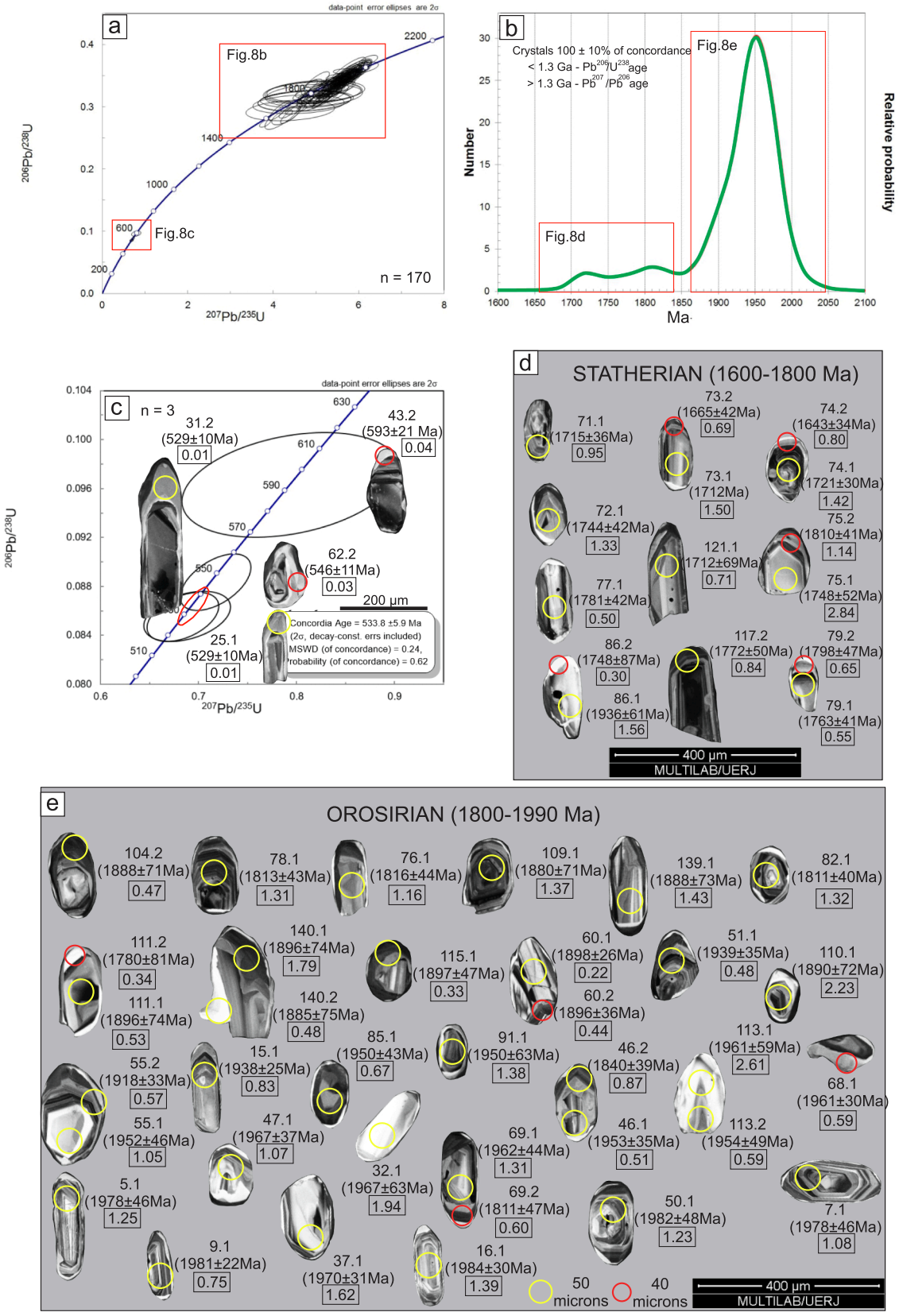

Fig. 8. (a) U-Pb Concordia diagram with all data for analyzed zircons from sample TH-34C (kyanite-orthoclase-garnet-biotite gneiss included in the Paleoproterozoic orthogneiss). (b) Relative age/probability density plot and histogram for the detrital zircon. (c) U-Pb Concordia diagram of spots in zircon metamorphic domains only. (d) and (e) Selected CL images with analyzed zircon spots for U–Pb. The numbers in rectangles represent Th/U ratios, bold numbers indicate the spot number and age. (d) Statherian zircon population. (e) Orosirian zircon population.

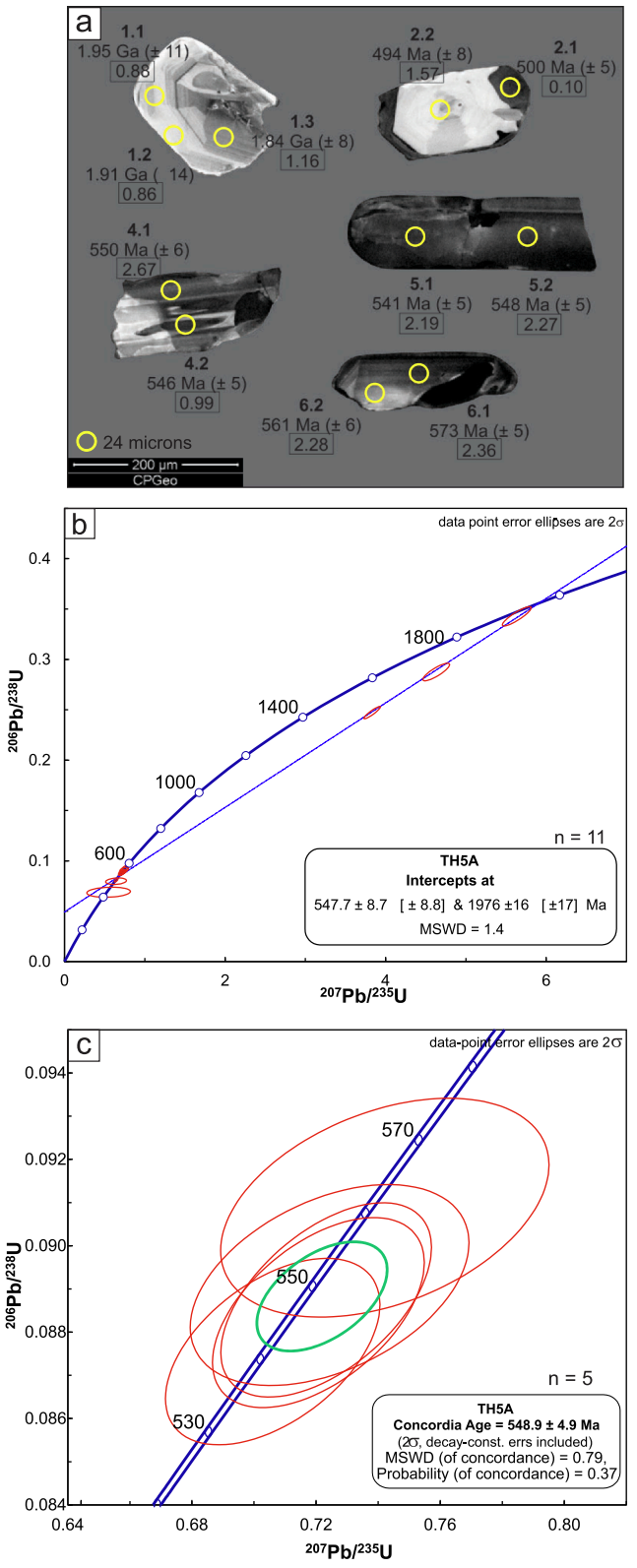

Fig. 9. CL image with 5 zircon crystals from sample TH-5A (Grt-Cpx-Amphibolite – José Gonçalves Suite), with indicated spots. The numbers in rectangles represent Th/U ratios, bold numbers indicate the spot number and the age. (b) U-Pb Concordia diagram with all data for analyzed zircon from sample TH-5A (Grt-Cpx-Amphibolite) aligned along in a discordia line. (c) Concordia age calculated for the red ellipses (550 Ma) representing spots #4.1, # 4.2, #5.1, #5.2 and #6.2.

ratios (2.28 to 2.36). The oscillatory zoning, interpreted as igneous, is disrupted by textural discontinuities along which the original zoning is resorbed, resulting in a dark gray rim that has not been dated (Fig. 9a).

Two spots were analyzed on grain 4 yielding ages of 550 ± 6 Ma and 546 ± 5 Ma with high Th/U ratios (2.67 to 0.99, respectively). The internal zircon structure shows a pattern of compositional sector zoning, typical of mafic rocks (Hoskin, 2000).

In grain 5, zoning is not well defined, yielding ages of 541 ± 5 Ma and 548 ± 5 Ma with high Th/U ratios (2.27 to 2.19, respectively). The absence of zoning could lead to the interpretation that it is metamorphic crystal but, the high Th/U ratios and the date of this grain are similar to the other grains (#4, #6), that show igneous internal structures, and are interpreted as igneous.

These spots produced a discordia with an upper intercept of 1976 ± 16 Ma and a lower intercept of 547.7 ± 8.7 Ma (Fig. 9b). A concordia mean age of 548.9 ± 4.9 Ma was calculated using only grains 4, 5 and 6 (Fig. 9c). Considering the high Th/U ratio and the absence of metamorphic overgrowths, the ca. 550 Ma age is interpreted as the timing of the mafic protolith crystallization. In this interpretation, the Paleoproterozoic grain 1 would be a xenocryst (Fig. 9a).

Contrastingly, crystal 2 displays a distinct internal structure and a younger age (Fig. 9a). Two spots reveal a $^{206}Pb/^{238}U$ age of 494 ± 8 Ma (core) and 500 ± 5 Ma (rim), overlapping in errors. The white to light gray core shows sector zoning and a Th/U ratio lower than the igneous grains (1.57). A dark gray rim cross cuts the sector zoning of the core and shows a very low Th/U ratio (Fig. 9a). A possible interpretation is that the core was cut by a newly grown domain (rim) of more homogeneous composition with Th/U ratio 0.1.

4.6. *Monazite U-Th-Pb data*

Monazite crystals from the two aluminous-paragneiss samples (TH-34C and TH-10A) were also dated by the chemical dating method. Crystals from the rock matrix and those included in garnet, were analyzed by electron microprobe. Major and trace elements analyses, as well as compositional maps of crystals, were generated (Y, Th, U and Ca – Figs. 10 and 12 and Supplementary Table 4). Some results were eliminated due to low/high sum of all analyzed elements (<98% and >102%) and/or low/high Si + P stoichiometric values (<0.9 and > 1.1).

4.6.1. *Kyanite-orthoclase-garnet-biotite gneiss (undetermined unit, sample TH-34C)*

Eighteen spots were measured on 10 monazite crystals, which are translucent, subhedral, rounded, with lengths between 31.6 and 91.5 µm, and show compositional zoning of Y, Th, U and Ca (Fig. 10a and 11a). Monazite grains are enriched in REE in relation to chondrite, and also in LREE in relation to HREE (Fig. 10b). This pattern of higher LREE and lower HREE is a typical characteristic of monazite grains (Bea, 1996). MREE and HREE patterns evidence greater scattering when compared to LREE (Fig. 10b). Cores and rims of monazite grains do not show significant variations in REE patterns. The analyzed monazite grains occur as inclusions in feldspar, quartz and biotite, and also in contact with garnet and zircon crystals. The variation of the mean dates seems to be linked to monazite location. Dates of monazite 6 and 11, in contact with garnet, are older (e.g., grain 6 with 552 ± 27 Ma, Fig. 10a, 10c and 11a), when compared to those in the matrix (e.g., 512 ± 25 Ma, Fig. 10 and 12a). Within a single grain measurement in the cores produce older dates than measurements in the rims, as expected (e.g., cores with 522 ± 28 Ma; rims with 503 ± 26 Ma, Fig. 10a). Grain 18, enclosed in an orthoclase crystal in the rock matrix, contains a Y-rich resorbed core with 570 ± 27 Ma and a Y-poor rim with 518 ± 22 Ma and 524 ± 28 Ma (Fig. 10a and 10e). Grain 13 has a Y-rich rim with 501 ± 27 Ma and 505 ± 26 Ma; it is in contact with a zircon crystal (Fig. 10a and 10d).

Based on these observations, two groups were defined: Group 1 with dates in the range 490 to 505 Ma (mean = 499 ± 9.3 Ma, Fig. 11b and 11c), representing 39% of the data obtained from the rims of matrix

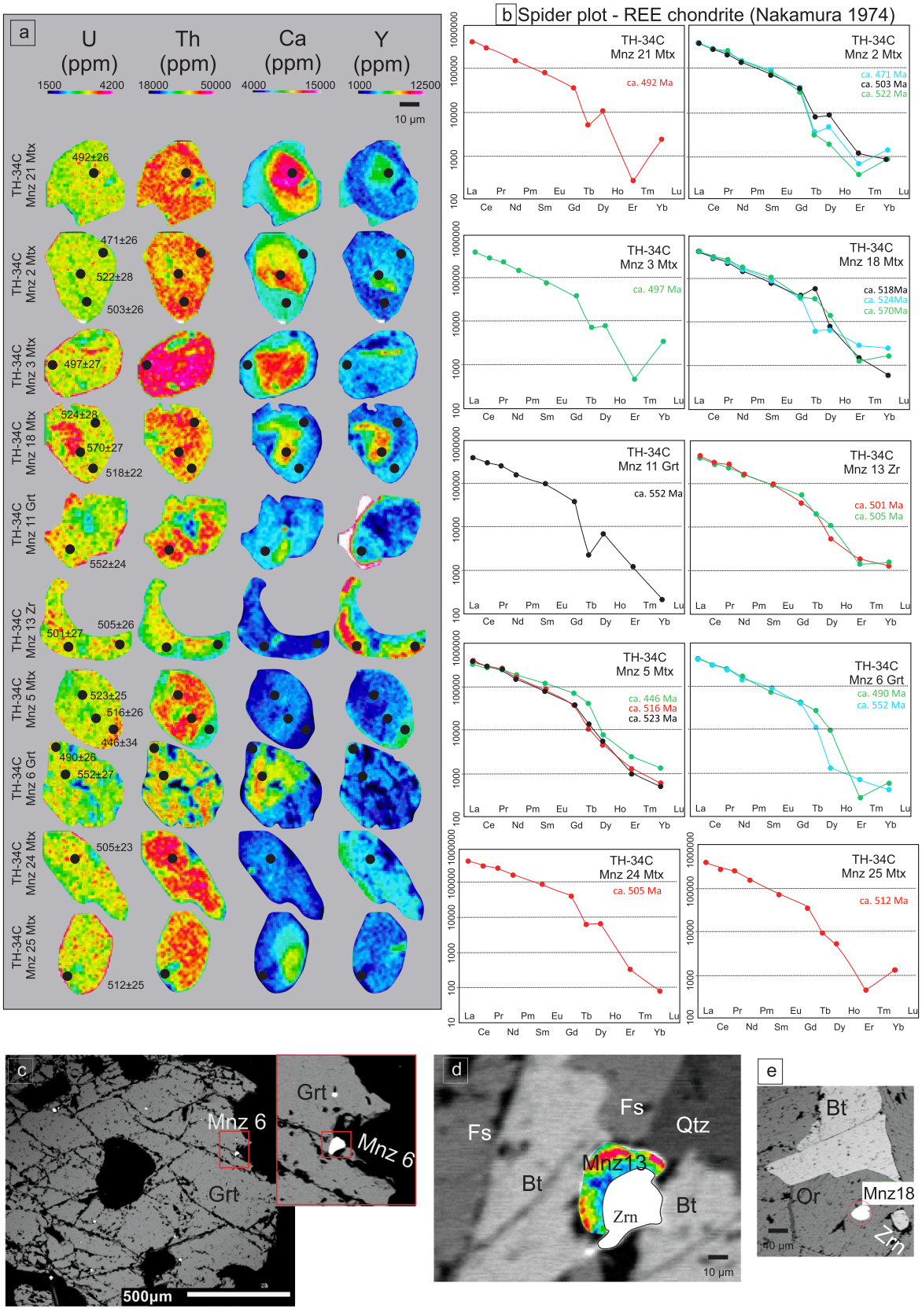

Fig. 10. (a) Representative compositional X-ray maps of monazite from sample TH-34C sample (kyanite- orthoclase-garnet-biotite gneiss which is included in Paleoproterozoic orthogneiss) with U, Th, Ca and Y in ppm. Black circles indicate spot analyses, with respective age in Ma. Notes on the left-hand side of the image designate the monazite identification and the textural context of the grains. (b) Monazite REE patterns normalized to the chondrite values of Nakamura (1974). Color- coded by corresponding ages (c) Mnz 6 Grt = monazite from matrix and in contact with garnet. (d) Mnz 13 Zr = monazite from matrix, included in biotite and in contact with zircon grain. (e) Mnz 18 Mtx = monazite from matrix and included in orthoclase.

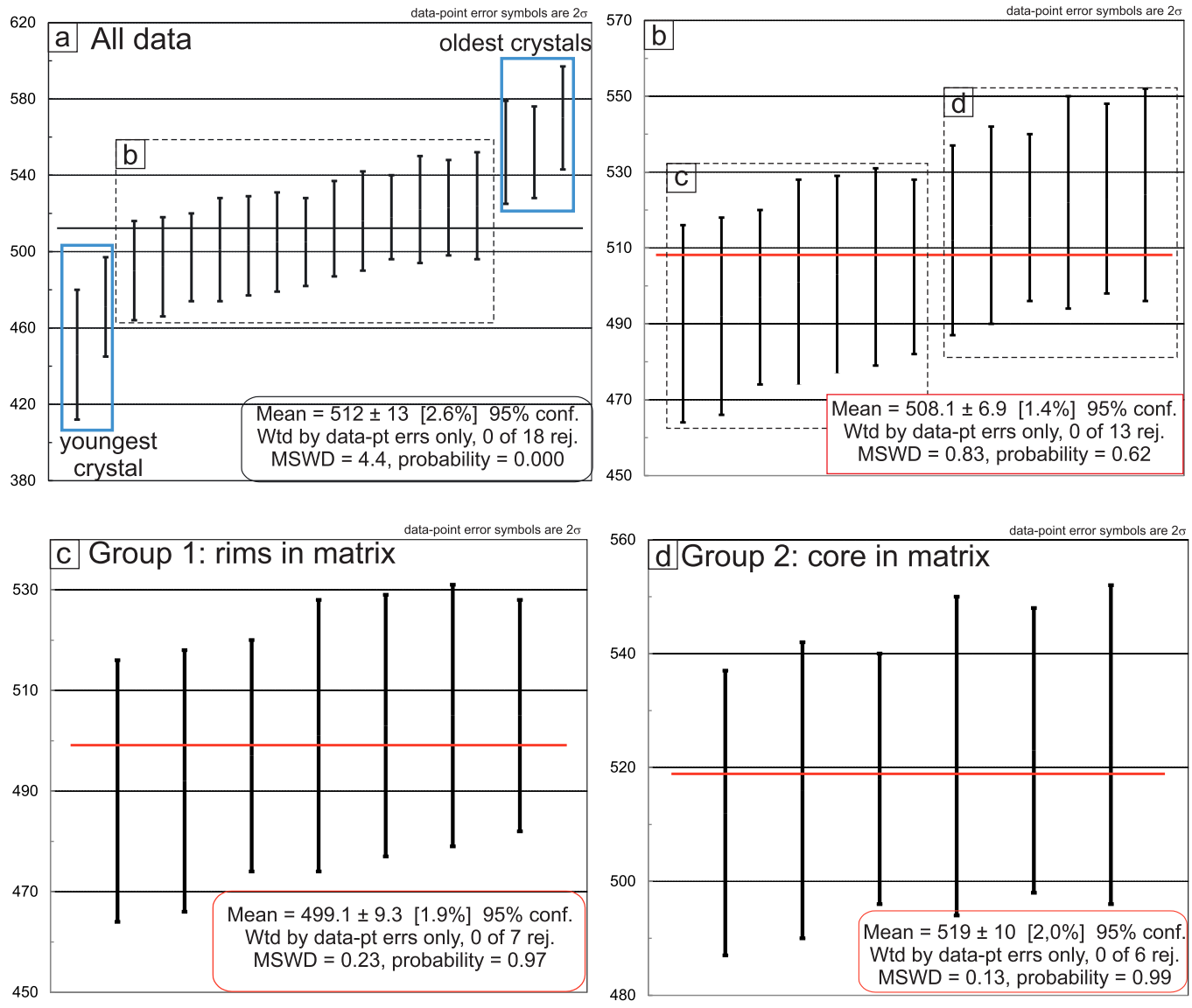

Fig. 11. Error-weighted average of U–Th–Pb_T EPMA ages of monazite for sample TH 34C (kyanite -orthoclase-garnet-biotite gneiss included in the Paleoproterozoic orthogneiss). Red lines show the mean values. Data-point error symbols are all 2 sigma. Wtd: weighted, conf.: confidence, rej.: rejected and MSWD: Mean Square of Weighted Derivates. (a) Data for all analyzed monazite grains from sample TH-34C (512 ± 13 Ma). Note that when the average includes all analyzes, the probability is low. (b) Data from all monazites in the center of the analysis, without the first two and the three-last recorded (508 ± 7 Ma). Note that the probability increases without these five samples. (c) Data from group 1, monazite rims from the matrix (499 ± 9.3 Ma). Probability increases even more when only this data is taken into account. (d) Data from group 2, monazite cores from the matrix (519 ± 10 Ma).

crystals (Fig. 10); Group 2 with dates in the range 512 to 524 Ma (mean = 519 ± 10 Ma, Fig. 11b and 11d), representing 33% of the data located both in cores and rims (Fig. 10). The younger and older monazite grains were studied separately: 446 ± 34 Ma and 471 ± 26 Ma (Fig. 11a) and 552 ± 24 Ma, 552 ± 27 Ma and 570 ± 27 Ma (Fig. 11a). Their significance is discussed below.

4.6.2. Kyanite-orthoclase-garnet-biotite granulite with retrometamorphic sillimanite (Búzios Succession, sample TH-10A)

Fifteen monazite crystals were analyzed in 52 spots (Fig. 13a). Crystals are translucent, rounded with diameters between 45 and 200 μm. MREE and HREE patterns reveal high scattering, but the LREE has a more regular pattern (Fig. 12b). The analyzed monazite grains are enriched in REE in relation to chondrite. The La and Yb contents are, respectively, ca. $4x10^5$ and 300 times greater than in chondrite (values of Nakamura, 1974 – Fig. 12b). This pattern observed in sample TH-10A, which has the highest LREE and the lowest HREE, is typical in monazites (Bea, 1996). Cores and rims of monazite crystals do not show significant variations in REE patterns. They occur in the matrix, in contact with garnet, zircon or apatite and included in garnet crystals. In general, the compositional zoning of Y, Th and Ca does not correlate with the measurements in the crystals (Fig. 12) with the exception of the uranium and yttrium content. There are two groups of monazite grains in which the dates are apparently related with the uranium concentration (Fig. 13a): Group A with U > 70,000 ppm, dates range from 400 to 480 Ma (mean = 469.6 ± 8.6 Ma, Fig. 13d), located in the rim of matrix grains and representing 27% of the total measurements; Group B with U less than 50,000 ppm, dates range from 490 to 540 Ma (mean = 512.4 ± 3.8 Ma, Fig. 13a), corresponding to 73% of the measurements. The latter group is subdivided in: Group B1 (510–490 Ma), with a mean age of 501.2 ± 5.8 Ma, obtained in rims, corresponding to 31% of all measurements (Fig. 13b), and Group B2 (510–540 Ma), with a mean age of 521.3 ± 5.2 Ma, obtained mostly in the monazite cores, representing 42% of the total measurements (Fig. 13c).

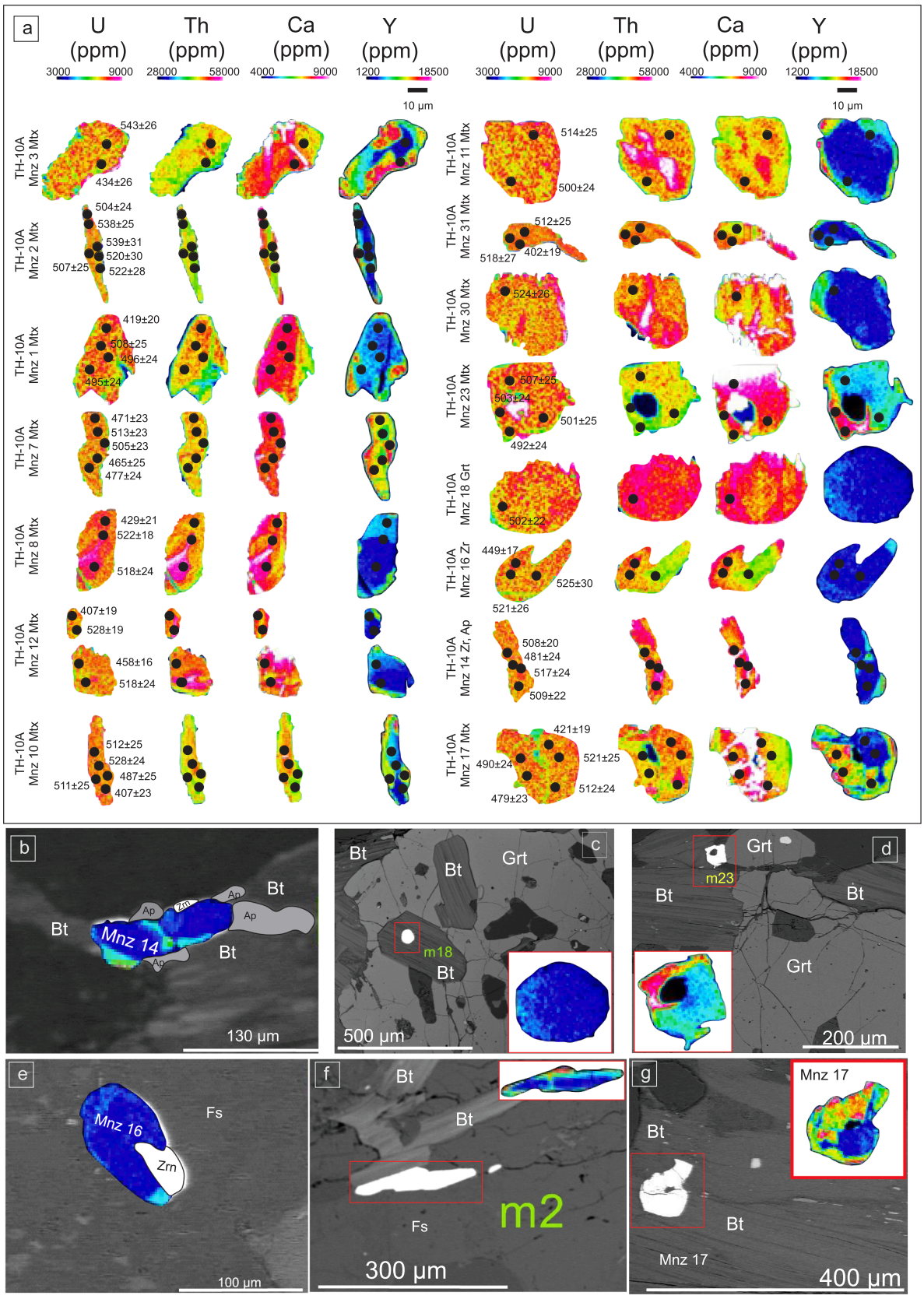

Fig. 12. (a) Representative compositional X-ray maps of monazite from sample TH-10A (kyanite-orthoclase-garnet-biotite granulite with retrometamorphic sillimanite from the Búzios Succession), with U, Th, Ca and Y in ppm. Black circles indicate spot analyses, with respective age in Ma. Notes on the left-hand side of the image designate the monazite identification and the textural context of the grain. (b) Mnz 14 Zr, Ap = monazite in contact with apatite and zircon. (c) Mnz 18 Grt = monazite included in garnet grain. (d) Mnz 23 Mtx = monazite in contact with garnet and biotite. (e) Mnz 16 Zr = Monazite included in feldspar and in contact with zircon. (f) Mnz 2 Mtx = monazite from matrix included in feldspar and in contact with biotite. (g) Mnz 17 Mtx = monazite from matrix included in biotite. (h) Monazite REE patterns normalized to the chondrite values of Nakamura (1974). Color- coded is by corresponding ages.

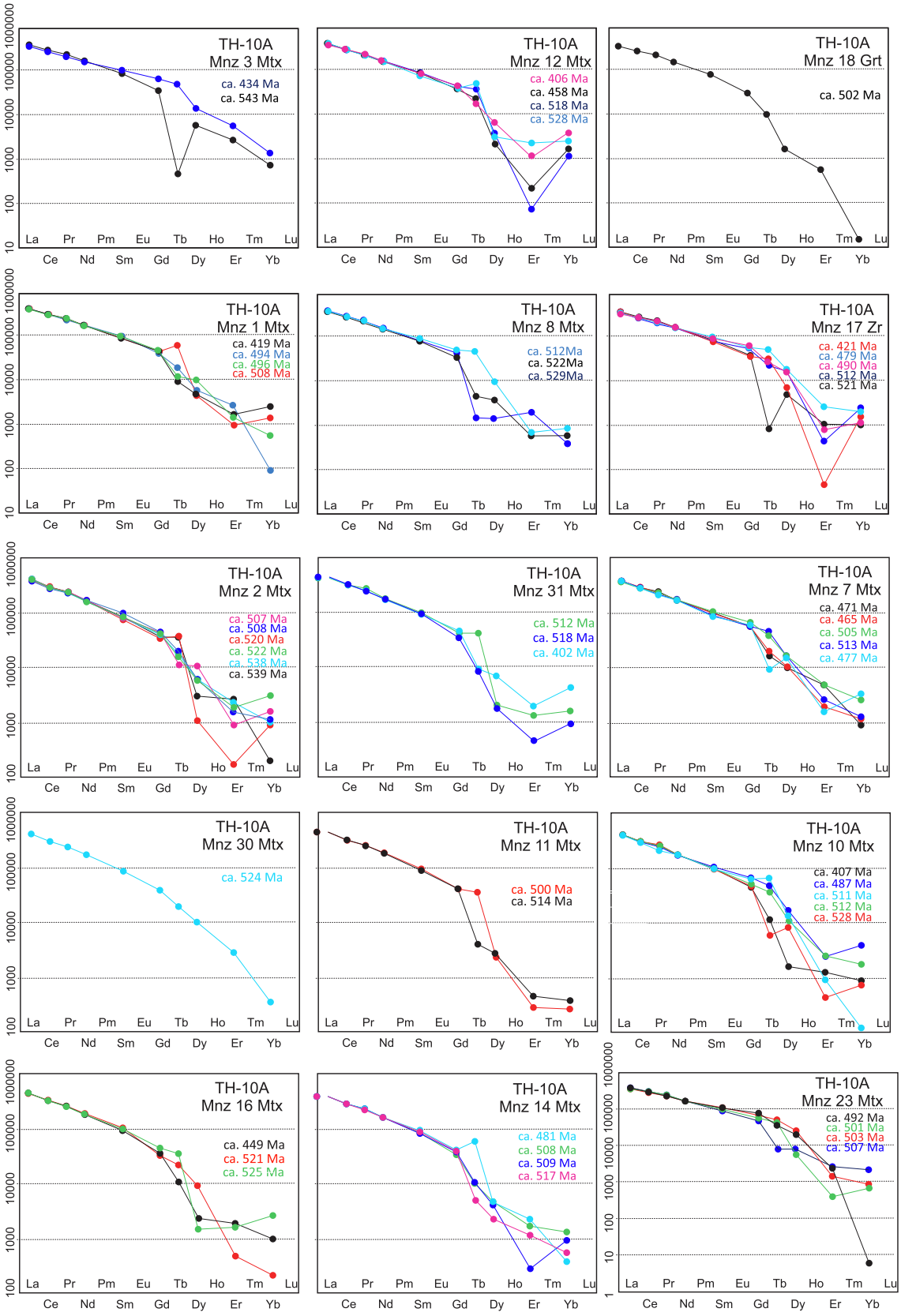

Fig. 12. (*continued*).

5. Discussion

According to the data presented here, the lithotypes enclosed in the Paleoproterozoic orthogneisses and the rock which represents the Búzios Succession show contrasting *P-T* conditions at their metamorphic near-peak. This is also evident from their distinct origins, ages, and tectonic

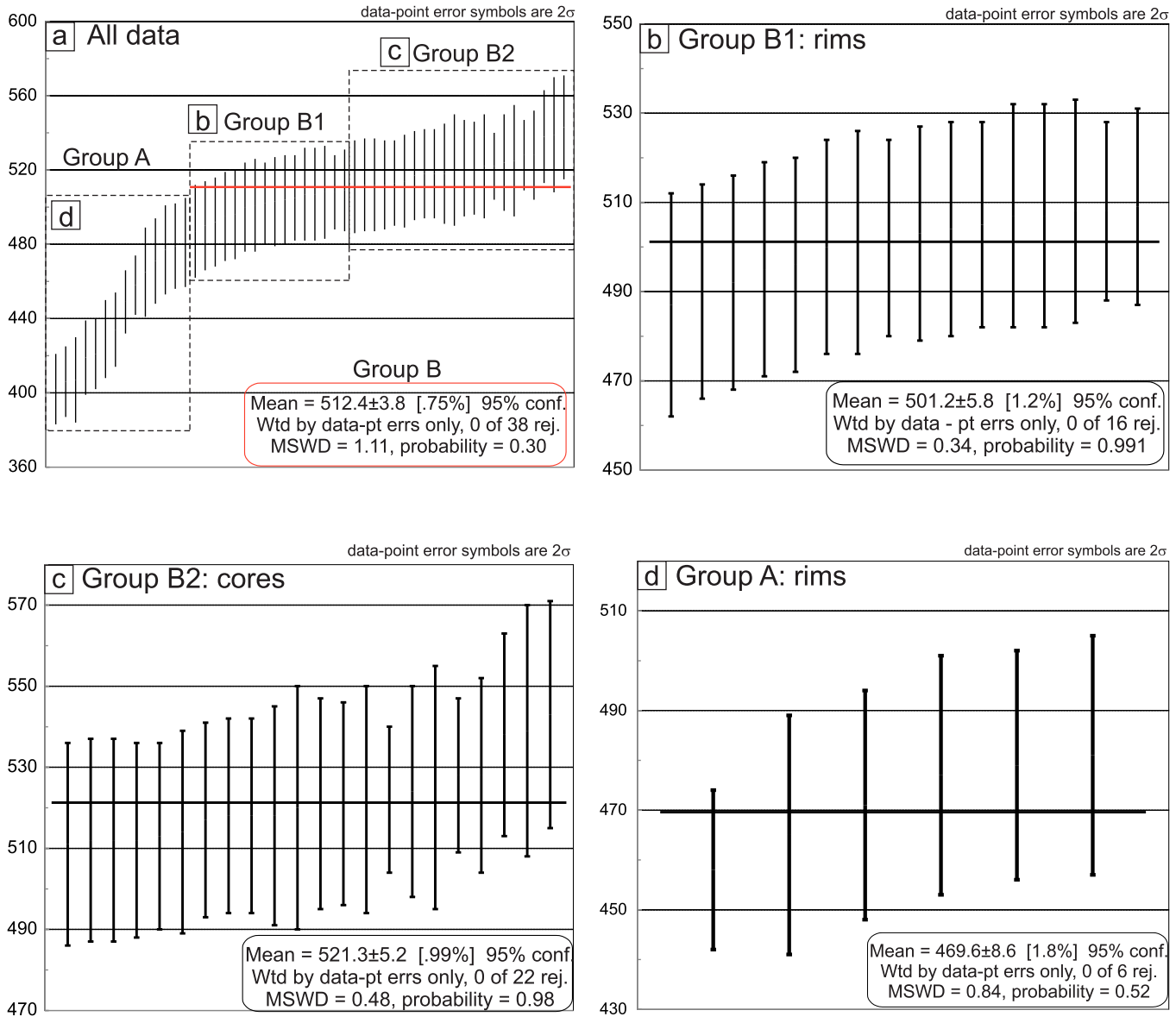

Fig. 13. Error-weighted average of U–Th–Pb_T EPMA ages of monazite for sample TH-10A (kyanite-orthoclase-garnet-biotite granulite with retrometamorphic sillimanite from the Búzios Succession). Red lines show the mean values. Data-point error symbols are all 2 sigma. Wtd: weighted, conf.: confidence, rej.: rejected and MSWD: Mean Square of Weighted Derivates. (a) All analyzed monazite from sample TH-10A. Only mean values for group B were calculated (512 ± 4 Ma). Note that when the average includes group B, the probability is low. (b) Data from group B1, monazite rims from the matrix (501 ± 6 Ma). Note that the probability increases. (c) Data from group B2, monazite cores from the matrix (521 ± 5 Ma). (d) Data from all younger monazite from the rims (470 ± 9 Ma).

evolution prior to their juxtaposition during the collisional event. We discuss here this contrasting evidence in the light of the tectono-metamorphic evolution of a convergent margin that ultimately resulted in a continental collisional orogen in the Ediacaran-Cambrian plate tectonic scenario.

5.1. *Protoliths – origin and age*

The Paleoproterozoic orthogneiss (Região dos Lagos Complex), that predominates in the Cabo Frio Tectonic Domain, contains numerous amphibolite lenses, with concordant deformational structures generated at amphibolite to granulite facies conditions (Fig. 4a and 6a). The age of these amphibolites was ill defined, as they were interpreted as tholeiitic basaltic paleodykes that intruded the orthogneisses between ca. 1.9 and 0.6 Ga (Schmitt et al., 2004; Schmitt et al., 2016). We provide better constraints to this issue, with the few zircon crystals obtained in the mafic rock sampled in a low strain domain (TH-5A). The internal zircon structure from sample TH-5A shows a pattern of compositional sector zoning, characteristic of mafic rocks (Hoskin, 2000). This author argues that broad zones in zircon crystals of mafic rocks tend to become progressively narrower during the magma evolution, generating concentric oscillatory zoning in higher silica magmas (e.g., granitoids). The concordant zircon grains (ca. 550 Ma – Fig. 9) are considered evidence to interpret these igneous domains as yielding the age of the mafic intrusion. The single Orosirian zircon, related to the upper intercept of the U-Pb discordia, is probably a xenocryst from the wall rock, incorporated in the mafic dyke during its emplacement. For this reason, the age of the mafic intrusions is interpreted to be Ediacaran (548.9 ± 4.9 Ma), early- to *syn*-collisional with respect to the Búzios Orogeny (see tectonic implications). Since these rocks were deformed and metamorphosed after the intrusion, the *P-T* conditions calculated could be extended to the wall rock, the Paleoproterozoic orthogneisses (Região dos Lagos Complex – Fig. 3b).

The kyanite-garnet-biotite gneiss lens is the first record of a

supracrustal unit within the Paleoproterozoic orthogneisses (sample TH-34C – Fig. 3f, 4c and 4d). U-Pb analyses on detrital zircon confirm that this sedimentary protolith has no contribution from Mesoproterozoic or Neoproterozoic sources (Figs. 8 and 14). For this reason, this protolith is not correlated with the Ediacaran paragneisses of the Búzios or Palmital successions, since their main detrital population is Neoproterozoic (Capistrano et al., 2020, Fernandes et al., 2015, Fig. 1b and 14). This 1.5 m thick lens is located inside a high strain migmatitic domain of the 2.0–1.9 Ga granitic and dioritic orthogneisses (Fig. 2). It could be either a xenolith or a sedimentary layer, tectonically interleaved during the orogenic event. Its major Paleoproterozoic detrital zircon population, with an age peak at ca. 1.95 Ga, has the same age as the surrounding igneous protoliths. Minor Statherian detrital zircon populations indicate additional younger sources, reported from the African side today (Fig. 1a – Kaoko belt and Angola Craton – Seth et al., 1998, Kröner et al., 2010). Hence this sedimentary lens cannot be a xenolith. It probably represents a younger sedimentary cover deposited on the Paleoproterozoic crust, its major source. The youngest detrital age of ca. 1.68 Ga marks the maximum sedimentation age. The 530 Ma metamorphic zircon rims limit the minimum depositional age.

Although the sedimentation age is poorly constrained, the absence of younger sources reinforces the idea that this sequence was not close to any Brasiliano-Pan-African orogen during its deposition (Fig. 1a). The predominant source was the Paleoproterozoic orthogneiss, that crops out today in the Cabo Frio Tectonic Domain (Brazilian SE coast) and in the Angola Craton (west Africa- Fig. 1a). This might represent a sedimentary basin deposited on the Angola Craton or on its proximal paleomargin. These data allied with the concordant deformational and migmatitic structures in the enclosed orthogneisses provide enough evidence to tie the *P-T* conditions calculated for this sample to the *P-T* conditions of the Paleoproterozoic orthogneisses, at least after ca. 1.68 Ga (Fig. 14).

Sample TH-10A, selected to represent the *P-T*-t path of the Búzios Succession, has a major Ediacaran detrital zircon population, and minor Tonian, Statherian and Neoarchean groups (Capistrano et al., 2020, Fernandes et al., 2015, Fig. 14). The Ediacaran detrital zircon grains represent sources predominantly juvenile to moderately evolved (ε_{Hf} between −4 and +10, Capistrano et al., 2020). According to these authors, this association is interpreted as an accretionary prism deposit developed prior to the Cambrian collision along with the juvenile mafic Ediacaran units (Fig. 2). The *P-T*-t path here determined will test this hypothesis.

5.2. Metamorphic P-T conditions

The samples related to the Paleoproterozoic orthogneiss (basement) show coherent *P-T* conditions. The mafic paleodyke (garnet-clinopyroxene amphibolite, sample TH-5A) provided a pressure of 10 ± 1 kbar and a temperature of 825 ± 46 °C. The paragneiss lens (kyanite-orthoclase-garnet-biotite gneiss – sample TH-34C) yielded a pressure of 10 ± 0.5 kbar and a temperature of 818 ± 70 °C, by THERMOCALC, and 750 °C by Zr-in-rutile. In addition, the hornblende-plagioclase thermometer applied on the dioritic orthogneiss (Região dos Lagos Complex) yielded temperatures between 759 °C and 772 °C, for samples TH-8A and TH-33B, respectively. These metamorphic values represent near-peak conditions attained in the Paleoproterozoic orthogneiss from the Região dos Lagos Complex.

The mafic paleodyke has a Grt + Cpx + Pl + Qtz-bearing assemblage that, according to Pattison (2003), might implies high pressure conditions of metamorphism in the transitional between amphibolite and granulite facies or between granulite and eclogite facies, at high temperatures. Although the Opx-free Grt + Cpx + Pl-bearing assemblage, as studied here, is characteristic of high-pressure metamorphism, it is not conclusive and not so effective to determine minimum temperature of formation, as Opx + Cpx + Pl-bearing assemblages (Pattison, 2003). Clinopyroxene emerges in the amphibolite facies, in both sillimanite and

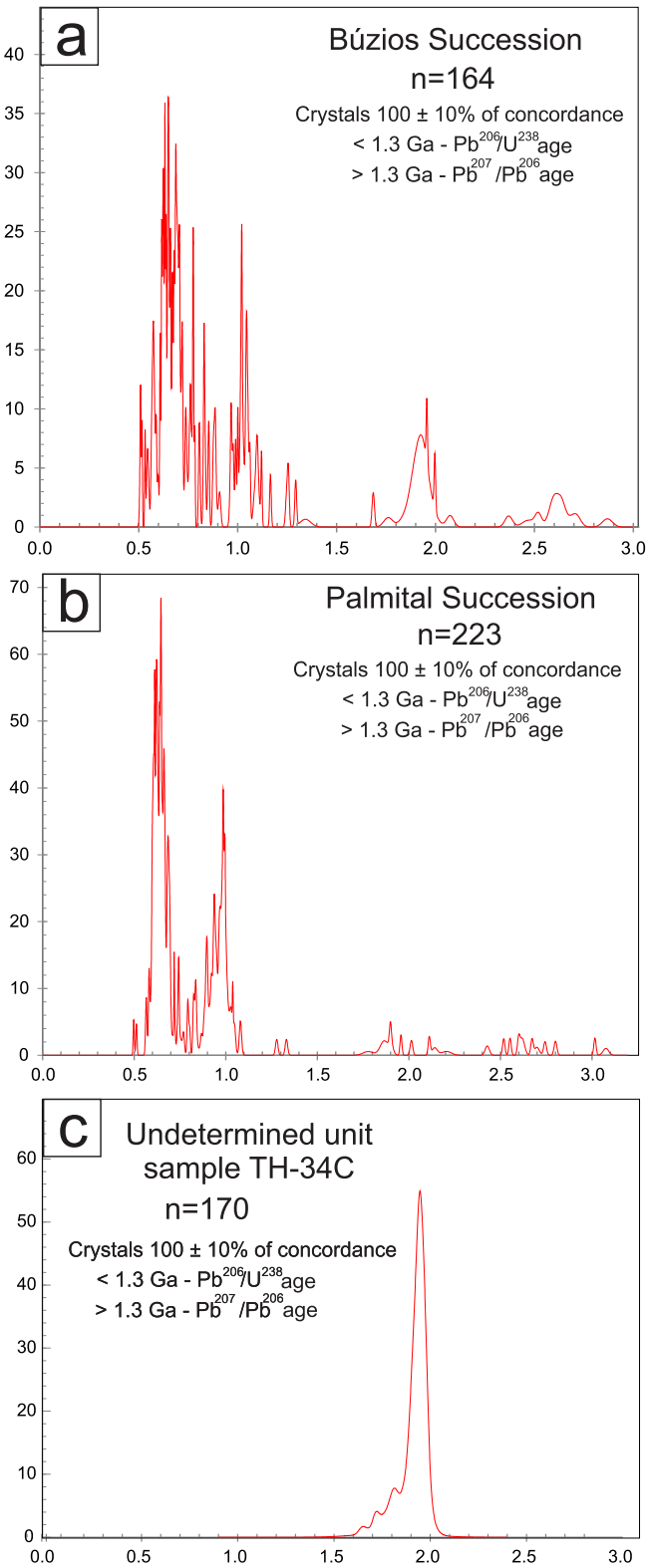

Fig. 14. The compiled published detrital zircon age data from the Búzios and Palmital Successions to compare with those of sample TH-34. (a) Relative age/probability density plot and histogram for the detrital zircon from the Búzios Succession (Capistrano et al., 2020; Fernandes et al., 2015). (b) Relative age/probability density plot and histogram for the detrital zircon from the Palmital Succession (Fernandes et al., 2015) (c) The range of detrital ages obtained for sample TH-34C, data from this work.

kyanite stability fields, with the onset of amphibole dehydration, starting at 650 °C (Bucher and Frey, 2002). A vast *P-T* window embraces the clinopyroxene coexistence with garnet and plagioclase. If quartz is added, the window is straitened, but it is still large and cannot be used alone as diagnostic of high-pressure granulite facies (Pattison, 2003). Therefore, clinopyroxene marks the beginning of the upper amphibolite facies (Bucher and Frey, 2002), and thus the mineral paragenesis Cpx + Grt + Pl should not be considered as diagnostic for granulite facies for the mafic igneous protoliths.

In mafic rocks, with increasing temperature, the hornblende decreases as the anhydrous granulite facies minerals substitute it progressively. Hornblende requires very high temperatures to be fully consumed. For this reason, many mafic granulites may still have prograde hornblende, as opposed to retrograde hornblende. Hence, the occurrence of prograde amphibole, in equilibrium with diopside and garnet, suggests that the granulite facies was attained in the studied rocks (TH-5A and 5B) and it confirms that the Cpx + Grt + Pl + Hbl is the peak paragenesis, which is consistent with the fact that anhydrous mafic granulite usually forms at temperatures above 850 °C (Patiño Douce and Beard 1995). The absence of orthopyroxene cannot be used as proof that the granulite facies has not been reached (Bucher and Frey, 2002). In the field, the garnet-clinopyroxene amphibolite (TH-5A and 5B) shows locally leucocratic veins, composed of plagioclase + quartz, surrounded by hornblende rich concentrates. These veins are interpreted as products of in situ partial melting and hence would represent leucosomes (Schmitt et al., 2004); they confirm the high temperature metamorphic conditions, ca. 800 °C, as calculated here.

The Búzios Succession, represented by the Ediacaran kyanite-orthoclase-garnet-biotite granulite with retrometamorphic sillimanite (sample TH-10A), reveals a distinct metamorphic path, with *P-T* near-peak conditions of 15.0 ± 0.6 kbar and 817 ± 24 °C. However, it shares similar characteristics with the kyanite-orthoclase-garnet-biotite gneiss included in the Paleoproterozoic orthogneiss (sample TH-34C). Both show the same metamorphic peak paragenesis, kyanite + orthoclase + garnet + biotite, with the absence of prograde muscovite and the evidence for partial melting showing that the reaction Ms + Pl + Qtz = Kfs + Ky + melt was been reached (Spear et al., 1999). But there are key chemical distinctions between these two samples. The lens of kyanite-orthoclase-garnet-biotite gneiss, enclosed in the Paleoproterozoic orthogneiss (sample TH-34C), has no variation in garnet composition, showing almost flat profiles, with slight increase of Fe and smooth decrease of Mg towards the rims (Fig. 5a). According to Spear (1991), caution is needed to interpret peak metamorphic temperatures in amphibolite facies, because of diffusion processes that may obliterate rim garnet composition during cooling. The calculation of the metamorphic peak temperatures of high grade is reliable but it becomes difficult if performed in terranes where cooling was slow, or on rocks with small garnets or wide $V_{garnet}/V_{biotite}$ ratio due to Fe-Mg exchange (Spear, 1991). By contrast, the kyanite- orthoclase-garnet-biotite granulite with retrometamorphic sillimanite from the Búzios Succession (sample TH-10A) shows significant variation of garnet composition from core to rim. The garnet porphyroblasts have cores enriched in Ca and Mg and poor in Fe, and rims enriched in Fe and poor in Ca and Mg. This variation could be interpreted as a record of growth during temperature increase due to progressive metamorphism (Spear, 1991).

Since Zr-in-rutile is a geothermometer less sensitive to cooling and independent of the Fe-Mg exchange of minerals, the temperatures calculated by this method can be considered as reliable (Tomkins et al., 2007). Luvizotto and Zack (2009) determined statistically that the highest Zr concentration values are better than the mean Zr concentrations for calculating peak temperatures. Zr-in-rutile provided a minimum metamorphic temperature of 747 ± 4 °C for the kyanite-orthoclase-garnet-biotite gneiss of the basement (sample TH-34C), similar to the one calculated by THERMOCALC (818 ± 70° C) considering the margin of error. The absence of sillimanite in the rock allows us to interpret the Zr-in-rutile result as the metamorphic peak temperature or the close to it. In the other sample (TH-10A), which represents the Búzios Succession, rutile is found as inclusion in garnet with minimal metamorphic temperatures of 783 ± 3 °C, also similar to the temperature calculated with THERMOCALC (817° ± 24 °C) for the metamorphic near-peak.

In a clockwise metamorphic return path, kyanite- orthoclase-garnet-biotite granulite with retrometamorphic sillimanite (sample TH-10A, Búzios Succession) developed sillimanite over relict crystals of kyanite (pseudomorphic texture), fibrolite intergrowth with biotite and some garnet grains partially replaced by symplectite (Grt + Kfs + Qtz + liquid = Bt + Sil, Spear et al., 1999). These *P-T* conditions were also calculated with THERMOCALC as 10.8 ± 0.7 kbar and 800 ± 27 °C. The temperature remained about equal, but the pressure dropped 5 kbar, characterizing an intense decompression, as suggested by Schmitt et al (2004).

5.3. Metamorphic P-T-t paths

P-T conditions are defined by chemical equilibria between different minerals while time is established by radioactive decay of elements such as U-Th to Pb in monazite and zircon. Nevertheless, the interpretation of their ages relative to the development of their host rock-forming minerals is a challenging task due to the complexities in the growth and dissolution behavior of these crystals.

The *P-T* data show that the metamorphic minerals from the rocks associated with the Paleoproterozoic orthogneiss are formed during the metamorphic near-peak at medium pressure and high temperature. On the other hand, the sample representing the Búzios Succession (Ediacaran supracrustal, TH-10A) shows a metamorphic near-peak at a higher pressure and temperature, followed by a second paragenesis related to a retrograde clockwise path linked to decompression (Fig. 6b). In this section, we incorporate textural observations with petrological, mineral chemistry and age data to establish the *P-T*-t paths for both basement and cover units.

The older metamorphic age obtained in a lens of paraderived rock included in Paleoproterozoic orthogneisses is preserved in three monazite crystals from the kyanite-orthoclase-garnet-biotite gneiss (sample TH-34) in the range of 570–550 Ma (Fig. 11a, 15a and 15b). There is no petrographic or isotopic evidence to justify presence of detrital monazite. Thus, we interpret that no detrital monazite grain survived the high-grade metamorphism, as also described by Williams (2001). Monazite can provide robust data for the beginning of high-grade metamorphism (Möller et al., 2003). It might preserve the age of prograde growth and, consequently, has the potential to provide the timing of high-grade metamorphism. Some authors point out that monazite in metapelites may originate in prograde metamorphism at lower to mid-amphibolite facies (500–600 °C) conditions (Bingen et al., 1996; Rubatto et al., 2001; Smith and van Barreiro, 1990) and it could preserve the age of growth up to ~850 °C assuming that dry conditions prevent recrystallization (Bingen and van Breemen, 1998). In addition, high-Y core represented by monazite number 18 (Fig. 10a, 10b and 10e – ca.570 Ma, #Mnz 18 Mtx) evidences that there was no capture of Y by the garnet (Pyle and Spear, 2003) and that, therefore, the garnet must have grown later, after ca. 570 Ma. Following this line of evidence, this older monazite preserved in the kyanite-orthoclase-garnet-biotite gneiss, enclosed in Paleoproterozoic orthogneiss (sample TH-34C), is interpreted to record the beginning of high-grade metamorphism along the prograde metamorphic path (Fig. 15a).

It is noteworthy that this older monazite age range overlaps with the crystallization age of the mafic paleodyke (sample TH-5A, ca. 550 Ma – Fig. 8). It is reasonable to assume that the dyke intruded the granitic orthogneiss when this was at least at a temperature of 550 °C, because this is the minimum temperature for crystallization of metamorphic monazite (Rubatto et al., 2001). This evidence would imply that the mafic dykes were emplaced at lower crustal levels, deeper than usually assumed for diabase dyke swarms. There are examples worldwide of basic dyke swarms emplaced at mid-crustal levels (Bright et al., 2014).

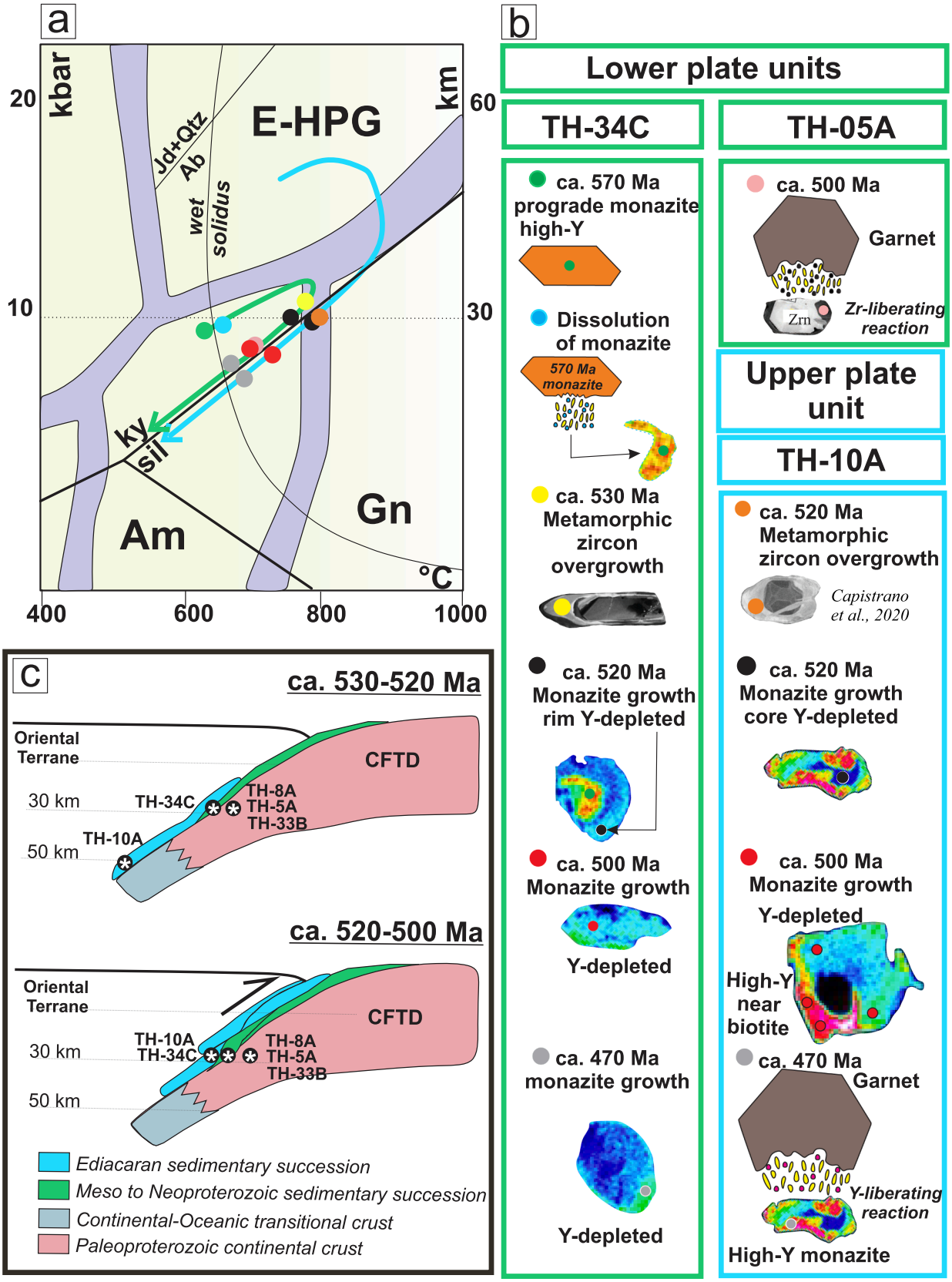

Fig. 15. (a) Pressure–temperature–time (*P-T-t*) paths of the analyzed samples based on textural relationships, thermobarometry, Zr-in-rutile thermometry and EPMA geochronology data of distinct monazite generations. This figure was constructed using the metamorphic facies division of Brown (2014). (b) Schematic diagram illustrating the crystallization sequence of zircon and monazite and its connection with the metamorphic stages recorded by studied rocks from the Cabo Frio Tectonic Domain. X-ray maps of the main monazite types and CL images of the main zircon are shown. (c) Schematic tectonic model with two orogenic stages: 530–520 Ma and 520–500 Ma. The tectonic position envisaged for the three analyzed samples is shown for each stage. E-HPG = Eclogite – High-P Granulite facies; Gn = Granulite facies; Am = Amphibolite facies.

The temperature difference between the mafic magma and the wall rock would be less than 500 °C, a possible reason for the preserved curved contacts among these two units in low strain domains (Fig. 3d). After the emplacement of the mafic paleodykes, our data shows that in in less than 20 m.y., these were submitted to the high-grade regional metamorphism, together with the wall rock (Paleoproterozoic orthogneiss), with near-peak pressure of 10 kbar and temperature of 825 °C.

The age of this metamorphic near-peak is obtained combining the monazite and zircon data. For Möller et al. (2003), monazite dating in metasedimentary rock is complementary to zircon dating, because monazite is less susceptible to inheritance from pre-metamorphic protoliths. According to Rubatto et al. (2001), the stability of zircon is defined by the presence of melt, with zircon and monazite crystallization, conserving a memory of long-lasting thermal events. In the kyanite-orthoclase-garnet-biotite gneiss (TH-34C, included in the Paleoproterozoic orthogneiss), metamorphic rims on zircons of 533 ± 8 Ma, provide the metamorphic age. Their Th/U ratios are below 0.3 and the cathodoluminescence images show typical metamorphic sector zonation (Fig. 9a). The low Th/U ratio is related to the presence of Th rich phases, such as monazite and metamorphic zircon in amphibolite and granulite facies rocks (Fraser et al., 1997; Kirkland et al., 2015; Rubatto, 2017). A more abundant group of monazite grains from the same rock yielded a mean age of 519 ± 10 Ma (Group 2, Fig. 12b and 12d). Considering that this group is only stable in the matrix, with grains concordant with the rock foliation and the fact that the zoned monazite grains show decrease in Y toward to rim (Fig. 10), we interpreted that monazite and garnet grew concomitantly (Fig. 15b). According to Pyle and Spear (2003), monazite is an accessory mineral that records interactions with garnet, both phases with high Y compatibility. During the growth of the garnet, Y is sequestered, affecting the monazite composition (Pyle and Spear, 2003). Hence, the diminution in Y in the direction of the rim, combined with the lack of monazite inclusions in garnet in sample TH-34C, suggest that monazite grew during the late stage of garnet growth and before garnet consumption (Fig. 15b). Since the monazite group, with mean age of 519 ± 10 Ma, grew concurrently with the metamorphic zircon rims (~530 Ma) with Th/U ratios below 0.1, we infer that the near-peak *P–T* conditions occurred between 530 Ma and 519 Ma (Fig. 15a and 15b). At approximately 530 Ma, the metamorphic zircon crystallized sequestering the HREE from the rock. Around 520–500 Ma when monazite crystallized, most of the HREE was already concentrated in the zircon. If zircon crystallization had not occurred at ca. 530 Ma, monazite grains would probably have a flatter HREE pattern (Fig. 10a and 10b).

A third group of monazite grains, from the same sample, provided a mean age of 499 ± 9.3 Ma (sample TH-34C), mainly analyzed in crystal rims from the matrix and Y-poor rims (Fig. 15a and 15b). Monazite 13 is an exception in this growth process; this grain is in contact with zircon with a Y-depleted rim and along the contact with biotite the grain has a high-Y rim (Fig. 10a and 10d). Apparently, there was no competition for HREE, that is, zircon did not affect the development of monazite grain nor its HREE profile (Fig. 10a, 10b and 10d). For this reason, the age of 499 ± 9.3 Ma was interpreted to register the retrograde path and cooling (Group 1, Fig. 12b and 12c, 15b). Additionally, the mafic paleodyke (TH-5A, garnet-clinopyroxene amphibolite), that intruded the basement at ca. 550 Ma, also registers this retrograde age in one concordant metamorphic zircon crystal of ca 500 Ma (Crystal 2, Fig. 8a). According to Yakymchuk et al. (2018) zircon with Th/U ratios <0.1 are expected to be metamorphic and zircon with Th/U ratios >0.1 could be igneous or metamorphic. According to this criterium both domains, core and rim from crystal 2, could be interpreted as metamorphic. This metamorphic zircon has a Th/U ratio higher than 0.1 (0.1 -rim and 1.57 – core), attributed primarily to the breakdown of Zr-bearing phases, due to a high-grade reaction probably related to partial melting by decompression followed by melt crystallization (Fraser et al., 1997; Kirkland et al.,2015; Rubatto, 2017). The variation of the Th/U ratios, higher in the core, and lower in the rim, might be related to a concomitant growth of a Th-rich mineral during the metamorphic event. Rubatto (2017) explains that the Th/U ratio of equilibrated zircon in these systems will be dependent on the amount of allanite or titanite and that zircon is commonly expected to have low Th/U ratios in allanite/titanite-bearing systems. In case of the studied rock, titanite is the Th-rich mineral. Following this statement, we suggest that at approximately 500 Ma there was Th competition in the system, possibly due to the growth of titanite, allowing zircon grain 2 to develop with a lower Th/U ratio than other crystals in the rock.

The sample representing the Búzios Succession (TH-10A, kyanite-orthoclase-garnet-biotite granulite with retormetamorphic sillimanite) has metamorphic zircon overgrowths in the age range of 530–508 Ma and Th/U ratios below 0.1, with a well-defined concordia age of 521 ± 11 Ma, interpreted as the metamorphic age (Capistrano et al., 2020). Its monazite data define two groups of ages: 521.3 ± 5.2 Ma (Group B2, Fig. 13a and 13c) and a 501.2 ± 5.8 Ma (Group B1, Fig. 13a and 13b). The first is interpreted as belonging to the near-peak metamorphism, since it is in agreement with the age of metamorphic zircon rims (Fig. 15b). According to Harley et al. (2007), when there is previous or concurrent growth of monazite, in which Th is a main component, this may lead to zircon with low Th concentration and consequently a low Th/U ratio. This is the case for sample TH-10A, with concurrent growth of monazite and zircon. It also exhibits a greater amount of metamorphic zircon overgrowths (Capistrano et al., 2020). As the stability of the zircon is defined by the presence of melt (Rubatto et al., 2001) and this rock reached high-grade metamorphic conditions (15 kbar and 800 °C), this might account for the abundance of metamorphic zircon rims in the paragneiss from the Búzios Succession when compared to the lens of paragneiss included in the Paleoproterozoic orthogneiss, which contains less metamorphic zircon rims.

The second group of monazite grains from the same sample, with age of 501.2 ± 5.8 Ma, shows high-Y rims mostly occurring in the matrix (Fig. 15b). These high -Y monazite domains could be correlated with the retrograde path, because of the reaction Bt + Sil partially replacing the garnet porphyroblasts (Fig. 4f). This reaction, involving also the consumption of K-feldspar and melt, is commonly associated with cooling (Spear et al., 1999). It is likely that these monazite rims are related with in-situ melt crystallization (Pyle and Spear, 2003). This would occur during the retrograde path generating partial melting and, thus, these monazites crystallized at ca. 500 Ma from that melt.

Therefore, the ca. 500 Ma age is correlated to the retrograde mineral assemblage in the Búzios Succession which developed at *P-T* conditions similar to the Paleoproterozoic orthogneiss and associated rocks. Since the same mineral metamorphic ages were obtained in the two samples related with the Paleoproterozoic orthogneiss (TH-34C and TH-5A), it can be assumed that at 500 Ma both, the Búzios Succession and the Região dos Lagos Complex were tectonically juxtaposed (Fig. 6 and 15c).

The ages here obtained for the Búzios Succession are coherent with previous published data. Metamorphic zircon grains from an interleaved Ediacaran mafic layer, in the same area, show a 530 Ma U-Pb concordia mean age (Capistrano et al., 2020). Schmitt et al. (2004) dated concordant zircons from a *syn*-D2 leucosome inside the Ediacaran paragneisses in Búzios at 525 ± 9 Ma (U-Pb with TIMS – Fig. 1b). Monazite ages from the same leucosomes range between 500 and 493 Ma, while monazite crystals from the paragneiss matrix yielded ages of 511 ± 2 Ma and 513 ± 2 Ma. For these authors, the 10 m.y. age gap between the leucosome and the metasedimentary rocks are linked to the origin of these monazites, the first group crystallized from a partial melt and the second group recrystallized in the solid state.

It is noteworthy in our data that both studied paragneiss samples presented Ordovician-Silurian monazites. The one related to the Búzios Succession has a monazite group with a mean age of 469.2 ± 8.6 Ma (Group A, Fig. 13a and 13d) that has mostly Y-rich rims likely linked to garnet breakdown. The paragneiss sample, included in Paleoproterozoic orthogneiss, shows two younger monazite crystals which have Y-poor rims (446 ± 34 Ma and 471 ± 26 Ma, Fig. 11a). The significance of these younger crystals is still a matter to be investigated. The heat produced as

effect of collision would have endured until 454 to 440 Ma and could also be correlated with the prominent magmatic intrusions in the adjacent Oriental Terrane (Fig. 1b – e.g., Bongiolo et al., 2015). These plutons are referred to as records of post collisional orogenic collapse (Valeriano et al., 2011).

6. Tectonic implications

This paper reports the highest pressure for Ediacaran-Cambrian metamorphic rocks within the Brasiliano-Pan African belts that crop out along the actual South Atlantic continental margins (Fig. 16). The inland branch of this orogenic system in Brazil, the Brasilia orogen, has many occurrences of metamorphic units formed at pressures higher than 10 kbar (Fig. 16). This belt is a product of convergence between the SW paleomargin of the São Francisco-Congo paleocontinent subducting below the Paranapanema paleocontinent, and the subsequent collision at 670–620 Ma (Campos Neto, 2000; Trouw et al., 2000, 2013; Fig. 1a and 16). The high-pressure units are located mainly in a nappe and associated klippen below the suture zone, and in the underlying nappes.

Within these nappes, the high pressures vary from 10 to 17 kbar with temperatures between 630 and 840 °C for the lower structural levels, and similar pressures but higher temperatures, ca. 800–960 °C for the upper levels, still within the lower plate, below the suture (Campos Neto and Caby, 1999, 2000; Campos Neto et al., 2010; Coelho et al., 2017; Garcia and Campos Neto, 2003; Trouw et al., 2013). One data gave a temperature of 1030 °C and pressure of 12 kbar, in the autochthonous suture zone (Rocha et al., 2017, Fig. 16).

In the Araçuaí-Ribeira orogenic system, there is only one occurrence of a metamorphic unit with pressure above 10 kbar. It is located in the Curitiba Terrane (Fig. 16), southern Ribeira belt, with pressure of 9–12 kbar at 670–810 °C (Faleiros et al., 2011, Fig. 16). The Curitiba Terrane is constituted of reworked Paleoproterozoic continental crust interleaved with Neoproterozoic metamorphic units. Ricardo et al. (2020) interpreted this medium to high pressure supracrustal unit as an accretionary prism sequence related to a subduction zone verging NW between the Luis Alves Craton and the Curitiba Terrane (Fig. 1a and 16). The occurrence of ophiolites marking this suture zone is also reported (Passarelli et al., 2018).

Our data is located within a context of a Paleoproterozoic continental crust (basement, Região dos Lagos Complex) reworked during the Brasiliano orogenies, tectonically interleaved with high-pressure Ediacaran units (cover, Búzios Succession – 15 kbar – this work). Along strike, these terranes (Cabo Frio and Curitiba) could be connected, but they are distant ca. 700 km and this connection is mostly covered by off shore South Atlantic Ocean sediments (Fig. 16). However, it is noteworthy that both are located at or near the contact with Neoproterozoic magmatic terranes to the NW (Fig. 16). Magmatic terranes correspond here to Neoproterozoic domains with voluminous batholiths of intermediate to acidic composition (Fig. 16). Along the contact with the Cabo Frio Tectonic Domain, the Costeiro Domain (part of the Oriental Terrane – Fig. 1b) is composed of Neoproterozoic ortho- and paragneisses. It is the locus for Late-Neoproterozoic to the Ordovician magmatic intrusions, considered a long-term high thermal flux terrane (Bento dos Santos et al., 2010, 2015).

Therefore, it makes sense to suggest that these medium to high pressure metamorphic occurrences, in the central and southern Ribeira belt, record ancient sutures zones that separate reworked Paleoproterozoic continental margin terranes and Neoproterozoic magmatic terranes (Fig. 16).

This observation can be confirmed by the example of the Brasília Belt. The Socorro-Guaxupé Nappe (numbers 6 and 7 – Fig. 16, e.g., Campos Neto and Caby, 1999, Reno et al., 2009, Rocha et al., 2017; Rocha et al., 2008) records UHT peak metamorphism under intermediate pressure conditions, with maximum pressures of ca. 12kbar in the Paragneiss metatexite unit (Rocha et al., 2017) and in the Basal Granulite unit (Del Lama et al., 2000; Campos Neto, 2000; Rocha et al., 2018). The high-pressure conditions within the Brasília Belt are recorded in the Andrelândia Nappe System (number 3 and 8 – Fig. 16, e.g.,

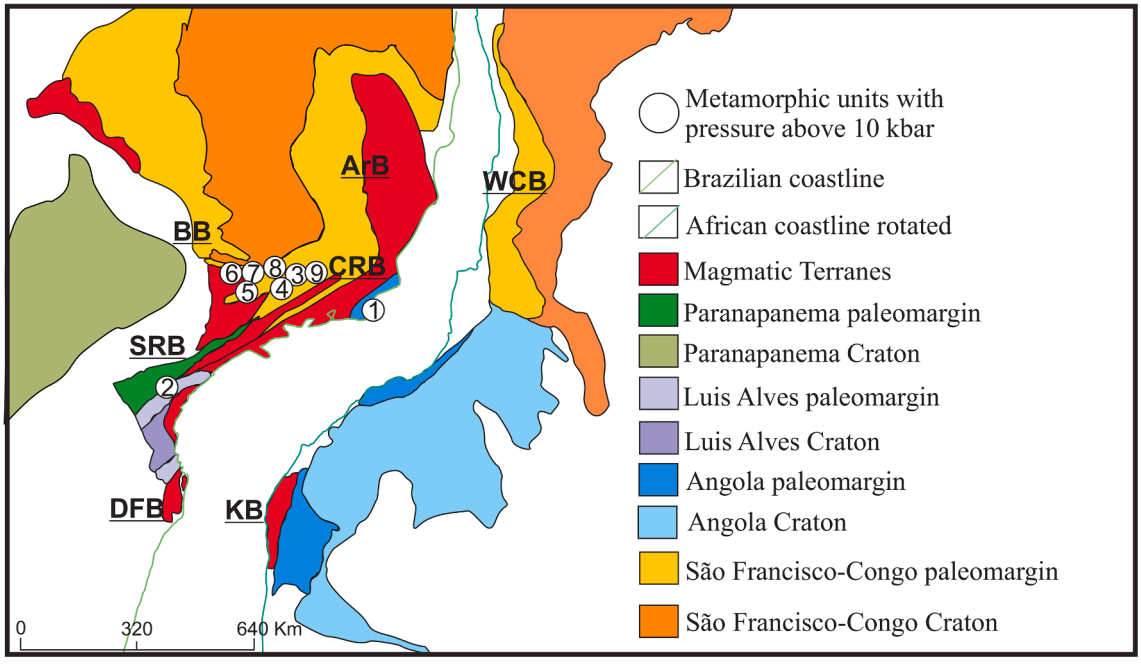

Fig. 16. South America and Africa continental margins reconstructed as Gondwana, according to Schmitt et al. (2018). Africa is rotated and South America is positioned in actual time. Coastlines are indicated. Mobile belts are: CRB - Central Ribeira belt, SRB - Southern Ribeira belt, BB - Brasília Belt, ArB -Araçuai belt, WCB – West Congo belt; KB – Kaoko belt, DFB – Dom Feliciano belt. Numbers indicate occurrence of metamorphic units with pressure above 10 kbar as published by: (1) Central Ribeira belt, Cabo Frio Tectonic Domain; our work; (2) Southern Ribeira belt, Curitiba terrane; Faleiros et al. (2011); (3) Brasília Belt, Liberdade Nappe; Coelho et al. (2017), Motta and Moraes (2017); (4) Brasília Belt, Luminárias Nappe; Fumes et al. (2019); (5) Brasília Belt, Pouso Alegre Complex; Cioffi et al. (2016) and Tedeschi et al. (2017); (6 and 7) Brasília Belt, Socorro-Guaxupé Nappe; Campos Neto and Caby (1999, 2000), Reno et al. (2009), Rocha et al. (2017); (8) Três Pontas-Varginha Nappe; Garcia and Campos Neto (2003); (9) Carvalhos Klippe; Campos Neto et al. (2010).

Campos Neto et al., 2010, Motta and Moraes, 2017), Três Pontas-Varginha Nappe (number 8 – Fig. 16, e.g., Garcia and Campos Neto, 2003), Carvalhos Klippe (number 9 – Fig. 16, e.g., Campos Neto et al., 2010), Liberdade Nappe (number 3 – Fig. 16; e.g., Coelho et al., 2017, Motta and Moraes, 2017). Therefore, the high pressures occurrences are located either along the contact with the Socorro-Guaxupé nappe or in the klippen and nappes further east (Fig. 16). Hence, it makes sense to compare this distribution with the conventional tectonic models where high-pressure units tend to indicate paleo-subduction zones.

Other evidence corroborates the hypothesis that the units here studied are related to a subduction-collision setting between the Cabo Frio Tectonic Domain and the Oriental Terrane of the Ribeira Belt (Fig. 1). The latter is a hot orogenic terrane, with magmatic units crystallized in the age range 630–480 Ma (Bento dos Santos et al., 2010, 2015; Bongiolo et al., 2016; Martins et al., 2016; Valeriano et al., 2011). Hence, it seems a good candidate to represent the upper plate of a subduction zone. Heilbron et al. (2008) defend a suture zone to the northwest of the Oriental Terrane, where a subduction zone pulls the São Francisco paleomargin towards southeast (the Occidental Terrane – Fig. 1a. However, there is no high-pressure unit in this proposed suture. Our data fit better with another suture zone, carrying the Angola continental paleomargin underneath the Oriental Terrane (Figs. 1, 15 and 16). To reinforce this, mafic layers interleaved with the Ediacaran supracrustal rocks (cover unit) are interpreted as oceanic crust based on geochemical and isotopic data (Capistrano et al., 2020). This sequence is interpreted by these authors as an ophiolite relic. Allied to this evidence, the contact between the Cabo Frio Tectonic Domain and the Oriental Terrane registers the strongest magnetic anomaly in the southeastern Brazilian continental crust (Stanton et al., 2010). These authors suggest that this anomaly might either represent a high strain zone or a suture zone or both. This orogenic suture zone extends offshore towards NE and SW to the Brazilian continental margin (Fig. 1). The fact that the Cabo Frio Tectonic Domain units record the youngest metamorphic peak ages in the Central Ribeira belt, defined as the Búzios orogeny, corroborates with the assumption that it marks the final collision in the West Gondwana amalgamation (Schmitt et al., 2016, 2018).

Considering all the data, this would be an appropriate region to test the possibility of tracking subduction zones in the Pan-African Brasiliano belts. We emphasize that in the Central Ribeira belt, this is the only occurrence that might record a suture zone. In the interval of 530–520 Ma, the basement and cover units had contrasting *P-T* paths and metamorphic peaks (Fig. 15). The major distinction is that the near-peak pressure reached 10 kbar in the former and 15 kbar in the latter, both at ca. 825–750 °C (Fig. 15).

One key question is how the Ediacaran sedimentary sequence, represented by the cover unit (Búzios Succession – sample TH-10A), has reached pressures of 15 kbar, buried into the lower crust, in less than 20 m.y (interval between the youngest detrital zircon – 550 Ma – and the oldest metamorphic rim – 530 Ma – Capistrano et al., 2020 and this paper). This pressure indicates that it was introduced c. 55 km down into the crust, considering a normal lithostatic gradient of 3.75 km/kbar. The most effective way to take a sedimentary succession to depths of 55 km is in a subduction zone (Stern, 2002). If we assume a subduction angle of 30°, the subduction rate would be 0.55 cm/yr. This is a very slow subduction rate according to Stern (2002), who considers a slab sinking vertically at 10 cm/yr as a fast rate. This corresponds to a subduction rate of 5.5 km/m.y., not even close to the slowest subduction zone rate recorded today in the Aegean Sea of 7.6 km/ m.y. (Syracuse et al., 2010). With this rate, at an angle of 30°, the cover unit would take 13 m.y. to reach 55 km depth.

If we change the subduction angle to 10°, the rate would increase to 1.58 cm/yr, still a low rate, implying that this rock unit would have to move more than 300 km in 20 m.y to reach 55 km vertical depth. This rate would be compatible with specific actual tectonic settings, with low angle or flat subduction, usually related with the arrival of a thicker oceanic crust in the trench (e.g., plateaus, volcanic island). Another mechanism to lower the subduction angle, is decreasing the density of the descending plate. This could happen with the arrival of a younger oceanic crust or a segment with a slab window, bringing transform-fracture zones or mid-ocean ridges to the trench (Groome and Thorkelson, 2009; Meneghini et al., 2014; Sisson et al., 2003). Both situations involve a less dense oceanic plate, due to a high geothermal gradient.

This leads to the second key question. If we consider that the cover unit went into a low angle subduction, taking 20 m.y. to reach the near pressure metamorphic peak of 15 kbar (Fig. 15), a temperature of ca. 800 °C is not expected. Usually in subduction zone models, at 50 km, the temperature of the subducting slab is between 200 and 500 °C (Stern, 2002). The conditions reached by the sample of this study are compatible with a normal continental crust gradient at depth of 55 km that corresponds to a pressure of 15kbar with temperature of approximately 800–900 °C. But as we mentioned earlier, there is no other mechanism able to bring this sedimentary sequence to this depth in less than 20 m.y. Therefore, the subduction channel here proposed must have an anomalous geothermal gradient, coherent with high temperature subduction, due to slab windows (Groome and Thorkelson, 2009). Slab breakoff is also a mechanism to explain high-temperature metamorphism by the relationship with advection heat passed by mafic magmatism (Santosh et al., 2012).

We record two lines of evidence that could be related to this environment. The occurrence of 550 Ma basaltic dykes intruding the Paleoproterozoic basement (our sample TH-5A) indicate that there was partial melt of mantle rocks in this pre- to *syn*-collisional setting. This would be compatible with an unusually high geothermal gradient. In addition, Capistrano et al. (2020) recognized also that the Ediacaran mafic gneisses interleaved with the metasedimentary rocks (cover unit) would represent an oceanic crust in a plume-related environment. This 580 Ma magmatic event occurred near or at the passive margin of the Angola Craton before convergence and collision with the Oriental Terrane. Therefore, this could justify the higher temperature in the subsequent subduction setting and even the hot orogenic nature of the Oriental Terrane, the upper plate of this subduction zone (Capistrano et al., 2020).

The hypothesis of NW-subduction of the Angola continental paleomargin below the Oriental Terrane of the Ribeira belt is also proposed in other papers (Martins et al., 2016; Schmitt et al., 2008, Capistrano et al., 2020). This is also consistent with the suggested tectonic setting for the Ediacaran high pressure metamorphic sequence from the Curitiba Terrane (Faleiros et al., 2011; Ricardo et al., 2020, Fig. 16).

The 520–500 Ma metamorphic zircon and monazite crystals from both basement and cover rocks are here interpreted as the timing that these distinct stratigraphic units were placed tectonically side by side during exhumation (Fig. 15). This is registered by the cover unit sample (TH-10A), that presents decompression from 15 to 10 kbar, between 520 and 500 Ma. The contrasting *P-T*-t path of basement and cover units is represented by an inverted metamorphic stratigraphy related to exhumation. The preservation of an inverted metamorphic stack indicates a fast exhumation rate, as the cover unit moves upwards at least 20 km within the crust, mostly by nappes displacement (Fig. 15).

Furthermore, the data here presented for the Central Ribeira belt corroborates with the broad and extensive geological evidence that excludes the intracontinental hypothesis suggested in recent papers for this Ediacaran-Cambrian tectonic setting (Fossen et al., 2020; Meira et al, 2015, 2019, 2020).

7. Conclusions

Geothermobarometric, U-Pb zircon and U-Pb-Th monazite data shown here, inserted in the evolutionary context of the Brasiliano orogeny, enable us to propose that during a first orogenic stage (530–520 Ma) the Região dos Lagos Complex (basement) and Búzios Succession (cover) were at distinct crustal levels. The Região dos Lagos Complex shows metamorphic near-peak conditions of 800–750 °C and

10 kbar, at a depth of at least 37 km in the transition zone between amphibolite and granulite facies. The Búzios Succession reached near-peak conditions of 15 kbar and 818 °C –785 °C at depths of at least 55 km in high-pressure granulite facies. On a clockwise return path, mainly related to decompression, this cover underwent retro-metamorphic conditions of 800 °C and 10 kbar during a second orogenic stage at 520–500 Ma.

This paper reports the highest pressure for Ediacaran-Cambrian metamorphic rocks within the Brasiliano-Pan African belts that crop out along the actual South Atlantic continental margins. It is probably a suture zone that separates a reworked Paleoproterozoic continental paleomargin and a Neoproterozoic magmatic terrane. Along strike, it connects with the Curitiba Terrane with a similar tectonic setting, comprising a Paleoproterozoic continental crust reworked in Brasiliano events and tectonically interleaved with even higher-pressure Ediacaran units also with pressure above 10 kbar. We propose that this suture represents an Ediacaran NW-subduction of the Angola continental paleomargin below the Oriental Terrane of the Ribeira belt. The 55 km burial of Ediacaran sediments (Búzios Succession) in 20 m.y. would be compatible with a low angle subduction zone active from 550 to 530 Ma. Intrusion of 550 Ma tholeiitic dykes within the Paleoproterozoic gneiss indicates a high geothermal gradient for this subduction setting, consistent with a low subduction rate.

The subduction theme is enigmatic and stimulating. Therefore, every new discovery adds constraints to the possible mechanisms involved. Our results encourage further studies with the purpose of improving the understanding of metamorphic evolution during the Pan-African Brasiliano event.

CRediT authorship contribution statement

Thayla Almeida Teixeira Vieira: Conceptualization, Methodology, Validation, Formal analysis, Investigation, Data curation, Writing – original draft, Writing – review & editing, Visualization, Project administration. **Renata da Silva Schmitt:** Conceptualization, Methodology, Validation, Investigation, Resources, Writing – original draft, Writing – review & editing, Visualization, Supervision, Project administration, Funding acquisition. **Julio Cezar Mendes:** Conceptualization, Methodology, Validation, Investigation, Data curation, Resources, Writing – review & editing, Visualization, Supervision, Project administration, Funding acquisition. **Renato Moraes:** Conceptualization, Validation, Resources, Formal analysis, Writing – review & editing, Visualization. **George Luiz Luvizotto:** Methodology, Validation, Resources, Investigation, Data curation, Writing – review & editing, Visualization. **Raphaela Lopes de Andrade Silva:** Conceptualization, Investigation, Writing – original draft, Visualization. **Rodrigo Vinagre:** Formal analysis, Writing – review & editing. **Silvia Regina de Medeiros:** Resources, Writing – review & editing, Funding acquisition.

Declaration of Competing Interest

The authors declare that they have no known competing financial interests or personal relationships that could have appeared to influence the work reported in this paper.

Acknowledgements

The authors thank the careful review of Prof. Dr. Rudolph Trouw (UFRJ) and all reviewers are similarly acknowledged here, Dr. Brenda C. Rocha and one anonymous. The authors acknowledge the Coordination for the Improvement of Higher Education Personnel (CAPES), the UFRJ, the Gondwana Project (CENPES-UFRJ- 13850) and the CNPq Universal project n. 1146 427676/2016-9 for the financial/logistical support. R.S. Schmitt and R. Moraes acknowledge the CNPq research grants n 311748/2018-0 and 305720/2020-1. We also are grateful to LABSONDA (UFRJ), MultiLab (UERJ) and LGPA (UERJ) for the technical support in the mineral chemistry and geochronological analysis. We also thank the collaboration in the field work of Gabriel Capistrano, Bernardo Khater, Úrsula Riente, Rodrigo Gentil, Julyanna Santos and Marina Kortchmar.

Appendix A. Supplementary data

Supplementary data to this article can be found online at https://doi.org/10.1016/j.precamres.2021.106479.

References

Alkmim, F.F., Pedrosa-Soares, A.C., Noce, C.M., Cruz, S.C.P., 2006. Sobre a evolução tectônica do orógeno Araçuaí-Congo Ocidental. Geonomos 15 (1), 25–43.
Bea, F., 1996. Residence of REE, Y5 Th and U in granites and grustal protoliths; implications for the chemistry of crustal melts. J. Petrol. 97 (3), 521–552.
Bento dos Santos, T., Munhá, J., Tassinari, C., Fonseca, P., Dias Neto, C., 2010. Thermochronology of central Ribeira Fold Belt, SE Brazil: petrological and geochronological evidence for high-temperature maintenance during Western Gondwana amalgamation. Precambr. Res. 180 (3–4), 285–298.
Bento dos Santos, T.M., Tassinari, C.C.G., Fonseca, P.E., 2015. Diachronic collision, slab break-off and long-term high thermal flux in the Brasiliano-Pan-African orogeny: implications for the geodynamic evolution of the Mantiqueira Province. Precambr. Res. 260, 1–22.
Bingen, B., Demaiffe, D., Hertogen, J., 1996. Redistribution of rare earth elements, thorium, and uranium over accessory minerals in the course of amphibolite to granulite facies metamorphism: the role of apatite and monazite in orthogneisses from southwestern Norway. Geochim. Cosmochim. Acta 60 (8), 1341–1354.
Bingen, B., van Breemen, O., 1998. U-Pb monazite ages in amphibolite- to granulite-facies orthogneiss reflect hydrous mineral breakdown reactions: Sveconorwegian Province of SW Norway. Contrib. Miner. Petrol. 132 (4), 336–353.
Black, L.P., Kamo, S.L., Allen, C.M., Davis, D.W., Aleinikoff, J.N., Valley, J.W., Mundil, R., Campbell, I.H., Korsch, R.J., Williams, I.S., Foudoulis, C., 2004. Improved $^{206}Pb/^{238}U$ microprobe geochronology by the monitoring of a trace-element-related matrix effect; SHRIMP, ID–TIMS, ELA–ICP–MS and oxygen isotope documentation for a series of zircon standards. Chem. Geol. 205 (1-2), 115–140.
Bongiolo, E.M., Renac, C., Piza, P.D.d.T., Schmitt, R.d.S., Mexias, A.S., 2016. Origin of pegmatites and fluids at Ponta Negra (RJ, Brazil) during late– to post–collisional stages of the Gondwana Assembly. Lithos 240-243, 259–275.
Bright, R.M., Amato, J.M., Denyszyn, S.W., Ernst, E.E., 2014. U-Pb geochronology of 1.1. Ga diabase in the southwest United States: testing models for the origin of a post Grenville large ignoues province. Lithosphere 6, 35–156.
Neves, B.B.d.B., Fuck, R.A., Pimentel, M.M., 2014. The Brasiliano collage in South America: a review. Braz. J. Geol. 44 (3), 493–518.
Brown, M., 2014. The contribution of metamorphic petrology to understanding lithosphere evolution and geodynamics. Geosci. Front. 5 (4), 553–569.
Bucher, K., Frey, M., 2002. Metamorphic rocks. Petrogenesis of Metamorphic Rocks. Springer, Berlin, Heidelberg.
Butler, R.W.H., 2018. Tectonic evolution of the Himalayan syntaxes: the view from Nanga Parbat. In: Treloar, P.J., Seale, M.P. (Eds.), Himalayan Tectonics: A Modern Synthesis. Geological Society, London, Special Publications, p. 483.
Campos Neto, M.C., 2000. Orogenic systems from southwestern Gondwana, an approach to Brasiliano-pan African Cycle and orogenic collage in southeastern Brazil. In: Cordani, U.G., Milani, E.J., Thomaz Filho, A. and Campos, D.A. (Eds.), Tectonic Evolution of South America. 31st International Geological Congress, Rio de Janeiro, Brazil, 335–365.
Campos Neto, M.d.C., Caby, R., 1999. Neoproterozoic high-pressure metamorphism and tectonic constraint from the nappe system south of the São Francisco Craton, southeast Brazil. Precambr. Res. 97 (1-2), 3–26.
da Costa Campos Neto, M., Caby, R., 2000. Terrane accretion and upward extrusion of high-pressure granulites in the Neoproterozoic nappes of southeast Brazil: Petrologic and structural constraints. Tectonics 19 (4), 669–687.
Neto, M.C.C., Figueiredo, M.C.H., 1995. The Rio Doce Orogeny, Southeastern Brazil. J. South Am. Earth Sci. 8 (2), 143–162.
Campos Neto, M.C., Cioffi, C.R., Moraes, R., Motta, R.G., Basei, M.A.S., 2010. Structural and metamorphic control on the exhumation of high-P granulite: The Carvalhos Klippe example, from the oriental Andrelândia Nappe System, southern portion of the Brasília Orogen, Brazil. Precambr. Res. 180, 125–142.
Capistrano, G.G., Schmitt, R.S., Medeiros, S.R., Fernandes, G.L.F., 2017. Evidence of a Neoproterozoic active continental margin – geochemistry and isotope geology of high-grade paragneiss from the Ribeira Orogen, SE Brazil. J. S. Am. Earth Sci. 77, 170–184.
Capistrano, G.G., Schmitt, R.S., Medeiros, S.R., Vieira, T.A.T., 2020. Ediacaran ophiolite relics in the SE Brazilian coast: Field, geochemical and geochronological evidence from metabasites and paragneisses. J. S. Am. Earth Sci. 105, 103040. https://doi.org/10.1016/j.jsames.2020.103040.
Cherniak, D.J., Watson, E.B., 2001. Pb diffusion in zircon. Chem. Geol. 172 (1-2), 5–24.
Cioffi, C.R., Campos Neto, M.C., Möller, A., Rocha, B.C., 2016. Paleoproterozoic continental crust generation events at 2.15 and 2.08 Ga in the basement of the southern Brasília Orogen, SE Brazil. Precambrian Res. 275, 176–196.
Coelho, M.B., Trouw, R.A.J., Ganade, C.E., Vinagre, R., Mendes, J.C., Sato, K., 2017. Constraining timing and P-T conditions of continental collision and late overprinting

in the Southern Brasília Orogen (SE-Brazil): U-Pb zircon ages and geothermobarometry of the Andrelândia Nappe System. Precambr. Res. 292, 194–215.
De Waele, B., Johnson, S.P., Pisarevsky, S.A., 2008. Palaeoproterozoic to Neoproterozoic growth and evolution of the eastern Congo Craton: Its role in the Rodinia puzzle. Precambr. Res. 160 (1-2), 127–141.
Del Lama, E.A., Zanardo, A., Oliveira, M.A.F., Morales, N., 2000. Exhumation of high-pressure granulites of the Guaxupé Complex, Southeastern Brazil. Geol. J. 35, 231–249.
Delor, C., Lafon, J.M., Rossi, P., Cage, M., Pato, D., Chevrel, S., Lê Metour, J., Matukov, D., Sergeev, S., 2006. Unravelling precambrian crustal growth of Central West Angola: Neoarchean to Siderian inheritance main Osirian accretion and discovery of the "Angolan" Panafrican Belt. In: 21st Colloquium of African Geology, Mocambique. Abstract Book, 40-41.
Donaldson, D.G., Webb, A.A.G., Menold, C.A., Kylanderclark, A.R.C. and Hacker, B.R., 2013. Petrochronology of Himalayan ultrahigh-pressure eclogite. Geology, 41, 835–838.
Elhlou, S., Belousova, E., Griffin, W.L., Pearson, N.J., O'reilly, S.Y., 2006. Trace element and isotopic composition of GJ-red zircon reference material by laser ablation. Goldschmidt Conference abstracts, A-5.
Faleiros, F.M., Campanha, G.A.C., Martins, L., Vlach, S.R.F., Vasconcelos, P.M., 2011. Ediacaran high-pressure collision metamorphism and tectonics of the southern Ribeira Belt (SE Brazil): evidence for terrane accretion and dispersion during Gondwana assembly. Precambr. Res. 189 (3-4), 263–291.
Fernandes, G.L.d.F., Schmitt, R.d.S., Bongiolo, E.M., Basei, M.A.S., Mendes, J.C., 2015. Unraveling the tectonic evolution of a Neoproterozoic-Cambrian active margin in the Ribeira Orogen (SE Brazil): U-Pb and Lu-Hf provenance data. Precambr. Res. 266, 337–360.
Fraser, G., Ellis, D., Eggins, S., 1997. Zirconium abundance in granulite facies minerals, with implications for zircon geochronology in high grade rocks. Geology 25 (7), 607–610.
Fonseca, M. J. G., Silva, Z. C, G, Campos, D.A., Tosatto, P., 1979. Folhas do Rio de Janeiro, Vitória e Iguape. Texto explicativo e Mapa. DNPM, Brasília, 239 p.
Fossen, H., Cavalcante, C., Konopásek, J., Meira, V.T., de Almeida, R.P., Hollanda, M.H. B.M., Trompette, R., 2020. A critical discussion of the subduction-collision model for the Neoproterozoic Araçuaí-West Congo orogen. Precambr. Res. 343, 105715. https://doi.org/10.1016/j.precamres.2020.105715.
Fumes, R.A., Luvizotto, G.L., Moraes, R., Heilbron, M., Vlach, S.R.F., 2019. Metamorphic modelling and petrochronology of metapelitic rocks from Luminárias Nappe, southern Brasília Belt (SE Brazil). Braz. J. Geol. 49 (2), 1–24.
Garcia, M.da.G.M., Neto, M.da.C.C., 2003. Contrasting metamorphic conditions in the Neoproterozoic collision-related nappes south of São Francisco Craton, SE Brazil. J. S. Am. Earth Sci. 15 (8), 853–870.
Gonçalves, G.O., Lana, C., Scholz, R., Buick, I.S., Gerdes, A., Kamo, S.L., Corfu, F., Marinho, M.M., Chaves, A.O., Valeriano, C., Nalini, H.A., 2016. An assessment of monazite from the Itambé pegmatite district for use as U-Pb isotope reference material for microanalysis and implications for the origin of the "Moacyr" monazite. Chem. Geol. 424, 30–50.
Groome, W.G., Thorkelson, D.J., 2009. The three-dimensional thermomechanical signature of ridge subduction and slab window migration. Tectonophysics 464 (1-4), 70–83.
Harley, S.L., Kelly, N.M., Moller, A., 2007. Zircon behaviour and the thermal histories of mountain chains. Elements 3 (1), 25–30.
Heilbron, M., Mohriak, W. U., Valeriano, C. M., Milani, E. J., Almeida, J., Tupinambá, M., 2000. From collision to extension: the roots of the Southeastern Continental Margin of Brazil. Atlantic Rifts and Continental Margins Geophysical Monograph 115.
Heilbron, M., Machado, N., 2003. Timing of terrane accretion in the Neoproterozoic-Eopaleozoic Ribeira belt SE Brazil. Precambr. Res. 125, 87–112.
Heilbron, M., Pedrosa-Soares, A.C., Campos Neto, M., Silva, L.C., Trouw, R.A.J., Janasi, V.C., 2004. A Província Mantiqueira. In: Mantesso-Neto, V., Bartorelli, A., Carneiro, C.D.R., Brito Neves, B.B. (Eds). O Desvendar de Um Continente: A Moderna Geologia da América do Sul e o Legado da Obra de Fernando Flávio Marques de Almeida, 203–234.
Heilbron, M., Valeriano, C.M., Tassinari, C.C.G., Almeida, J.C.H., Tupinambá, M., Siga Jr., O., Trouw, R.A.J., 2008. Correlation of Neoproterozoic terranes between the Ribeira Belt. SE Brazil and its African counterpart: comparative tectonic evolution and open questions. In: Pankhurst R.J., Trouw R.A.J., Brito Neves B.B., De Wit M.J. (eds.), West Gondwana Pre-Cenozoic Correlations Across the South Atlantic Region. Geological Society, London, Special Publications, 294, 279–296.
Heilbron, M., Tupinambá, M., Valeriano, C.de.M., Armstrong, R., do Eirado Siva, L.G., Melo, R.S., Simonetti, A., Pedrosa Soares, A.C., Machado, N., 2013. The Serra da Bolívia Complex: the record of a new Neo-proterozoic arc-related unit at Ribeira Belt. Precambr. Res. 238, 158–175.
Herwegh, M., Pfiffner, O.A., 2005. Tectono-metamorphic evolution of a nappe stack: a case study of the Swiss Alps. Tectonophysics 404 (1-2), 55–76.
Holland, T., Blundy, J., 1994. Non-ideal interactions in calcic amphiboles and their bearing on amphibole-plagioclase thermometry. Contrib. Miner. Petrol. 116 (4), 433–447.
Hoskin, P.W.O., 2000. Patterns of chaos: fractal statistics and the oscillatory chemistry of zircon. Geochim. Cosmochim. Acta 64 (11), 1905–1923.
Kirkland, C.L., Smithies, R.H., Taylor, R.J.M., Evans, N., McDonald, B., 2015. Zircon Th/U ratios in magmatic environs. Lithos 212-215, 397–414.
Kröner, A., Rojas-Agramonte, Y., Hegner, E., Hoffmann, K.-H., Wingate, M.T.D., 2010. SHRIMP zircon dating and Nd isotopic systematics of Palaeoproterozoic migmatitic orthogneisses in the Epupa Metamorphic Complex of northwestern Namibia. Precambr. Res. 183 (1), 50–69.
Ludwig, K., 2009. SQUID 2: A User's Manual. Berkeley Chronology Center Special Publication, p. 110, 5.
Luvizotto, G.L., Zack, T., 2009. Nb and Zr behavior in rutile during high–grade metamorphism and retrogression: an example from the Ivrea-Verbano Zone. Chem. Geol. 261 (3-4), 303–317.
Luvizotto, G.L., Zack, T., Triebold, S., von Eynatten, H., 2009. Rutile occurrence and trace element behavior in medium-grade metasedimentary rocks: example from the Erzgebirge, Germany. Mineral. Petrol. 97 (3-4), 233–249.
Martins, G.G., Mendes, J.C., Schmitt, R.S., Armstrong, R., Valeriano, C.M., 2016. 550–490 Ma pre-to post-collisional shoshonitic rocks in the Ribeira Belt (SE Brazil) and their tectonic significance. Precambr. Res. 286, 352–369.
Meira, V.T., García-Casco, A., Juliani, C., Almeida, R.P., Schorscher, J.H.D., 2015. The role of intracontinental deformation in supercontinent assembly: insights from the Ribeira Belt, Southeastern Brazil (Neoproterozoic West Gondwana). Terra Nova 27 (3), 206–217.
Meira, V.T., García-Casco, A., Hyppolito, T., Juliani, C. Schorscher, J.H.D., 2019. Tectono-metamorphic evolution of the Central Ribeira Belt, Brazil: A case of late Neoproterozoic intracontinental orogeny and flow of partially molten deep crust during the assembly of West Gondwana. Tectonics 38 (8), 3182–3209.
Meira, V.T., García-Casco, A., Hyppolito, T., Juliani, C. Schorscher, J.H.D., 2020. Reply to comment by Heilbron and Valeriano on "Tectono metamorphic evolution of the Central Ribeira Belt, Brazil: A case of late Neoproterozoic intracontinental orogeny and flow of partially molten deep crust during the assembly of West Gondwana. Tectonics 39 (7), e2020TC006307.
Mendes J. C., Schmitt R.S., Penha H.M., Ludka I.P., Dantas, E. L., 2006. Calc-alkaline magmatism in a low pressure high temperature Neoproterozoic terrane, SE Brazil: new U-Pb data. In: V Simposio Sudamericano de Geologia Isotopica, 2006, Punta del Este. Short papers of the V SSAGI, 2006. v. 1. p. 123–125.
Meneghini, F., Kisters, A., Buick, I., F. Åke., 2014. Fingerprints of late Neoproterozoic ridge subduction in the Pan-African Damara belt, Namibia. Geology, 42 (10) 903–906.
Möller, A., Hensen, B.J., Armstrong, R.A., Mezger, K., Ballèvre, M., 2003. U-Pb zircon and monazite age contraints on granulite-facies metamorphism and deformation in the Strangways Metamorphic Complex (central Australia). Contrib. Miner. Petrol. 145, 406–423.
Möller, C., Majka, J., Janák, M., van Roermund, H., 2018. High- and ultrahigh-pressure rocks—keys to lithosphere dynamics. J. Metamorph. Geol. 36 (5), 511–515.
Monié, P., Bosch, D., Bruguier, O., Vauchez, A., Rolland, Y., Nsungani, P., Buta Neto, A., 2012. The Late Neoproterozoic/Early Palaeozoic evolution of the West Congo Belt of NW Angola: geochronological (U-Pb and Ar-Ar) and petrostructural constraints. Terra Nova 24 (3), 238–247.
Moraes, R., Brown, M., Fuck, R.A., Camargo, M.A., Lima, T.M., 2002. J. Petrol. 43, 1673–1705.
Motta, R. G. and Moraes, R., 2017. Pseudo- and real-inverted metamorphism caused by the superposition and extrusion of a stack of nappes: a case study of the Southern Brasília Orogen, Brazil. Int. J. Earth Sci., 106 (7), 2407–2427.
Passarelli, C.R., Basei, M.A. S., Siga, O., Harara, O.M.M., 2018. The Luis Alves and Curitiba Terranes: Continental Fragments in the Adamastor Ocean. In: Geology of Southwest Gondwana. Springer, Cham, pp. 189–215.
Patiño Douce, A.E., Beard, J.S., 1995. Dehydration Melting of biotite gneiss and quartz amphibolite from 3 to 15 kbar. Journal of Petrology 36:(3) 707-738.
Pattison, D.R.M., Chacko, T., Farquhar, J., McFarlane, C.R.M., 2003. Temperatures of granulite-facies metamorphism: constraints from experimental phase equilibria and thermobarometry for retrograde exchange. J. Petrol. 44 (5), 867–900.
Pattison, D.R.M., 2003. Petrogenetic significance of orthopyroxene-free garnet + clinopyroxene + plagioclase-bearing metabasites with respect to the amphibolite and granulite facies. J. Metamorph. Geol. 21, 21–34.
Peixoto, C., Heilbron, M., Ragatky, D., Armstrong, R., Dantas, E., Valeriano, C., Simonetti, A., 2017. Tectonic evolution of the Juvenile Tonian Serra da Prata magmatic arc in the Ribeira belt, SE Brazil: Implications for early west Gondwana amalgamation. Precambr. Res. 302, 221–254.
Powell, R., Holland, T.J.B., 1994. Optimal geothermometry and geobarometry. Am. Mineral. 79, 120–133.
Pyle, J.M., Spear, F.S., 2003. Four generations of accessory phase growth in lowpressure migmatites from SW New Hampshire. Am. Mineral. 88, 338–351.
Reno, B.L., Brown, M., Kobayashi, K., Nakamura, E., Piccoli, P.M., Trouw, R.A.J., 2009. Eclogite-high-pressure granulite metamorphism records early collision in West Gondwana: new data from the Southern Brasília Belt, Brazil. J. Geol. Soc., London 166, 1013–1032.
Ricardo, B.S., Faleiros, F.M., Moraes, R., Siga O.J., Campanha, G.A.C., 2020. Tectonic implications of juxtaposed high- and low-pressure metamorphic field gradient rocks in the Turvo-Cajati Formation, Curitiba Terrane, Ribeira Belt, Brazil. Precambr. Res., 105766.
Rocha, B.C., Moraes, R., Möller, A., Cioffi, C.R., Jercinovic, M.J., 2017. Timing of anatexis and melt crystallization in the Socorro-Guaxupé Nappe, SE Brazil: insights from trace element composition of zircon, monazite and garnet coupled to U—Pb geochronology. Lithos 277, 337–355.
Rocha, B.C., Moraes, R., Möller, A., Cioffi, C.R., 2018. Magmatic inheritance vs. UHT metamorphism: Zircon petrochronology of granulites and petrogenesis of charnockitic leucosomes of the Socorro-Guaxupé nappe, SE Brazil. Lithos 314, 16–39.
Rubatto, D., Williams, I., Buick, I., 2001. Zircon and monazite response to prograde metamorphism in the Reynolds Range, central Australia. Contrib. Miner. Petrol. 140, 458–468.
Rubatto, D., 2002. Zircon trace element geochemistry: partitioning with garnet and the link between U-Pb ages and metamorphism. Chem. Geol. 184, 123–138.

Rubatto, D., 2017. Zircon: the metamorphic mineral. Rev. Mineral. Geochem. 83, 261–296.
Santosh, M., Liu, S.J., Tsunogae, T., Li, J.H., 2012. Paleoproterozoic ultrahigh temperature granulites in the North China Craton: implications for tectonic models on extreme crustal metamorphism. Precambr. Res. 222–223, 77–106.
Sato, K., Tassinari, C. C. G., Basei, M. A. S., Júnior, O. S., Onoe, A. T., Souza, M. D., 2014. Sensitive High Resolution Ion Microprobe (SHRIMP IIe/MC) of the Institute of Geosciences of the University of São Paulo, Brazil: analytical method and first results. Geologia USP, Série científica, São Paulo, v. 14, n. 3, p. 3–18.
Schmitt, R.S., Trouw, R.A.J., Van Schmus, W.R., Pimentel, M.M., 2004. Late amalgamation in the central part of West Gondwana: new geochronological data and the characterization of a Cambrian collisional orogeny in the Ribeira Belt (SE Brazil). Precambr. Res. 133, 29–61.
Schmitt, R.S., Trouw, R.A.J., Medeiros, S.R., Dantas, E.L., 2008. Age and geotectonic setting of a Late-Neoproterozoic amphibolithe and paragneiss association from southeastern Brazil based on geochemistry and Sm-Nd data. Gondwana Res. 13, 502–515.
Schmitt, R.S., Trouw, R.A.J., Van Schmus, W.R., Passchier, C.W., 2008b. Cambrian orogeny in the Ribeira Belt (SE Brazil) and correlations within West Gondwana: ties that bind underwater. In: Pankhurst R.J., Trouw R.A.J., Brito Neves B.B., De Wit M.J. (eds.) West Gondwana: PreCenozoic Correlations across the South Atlantic Region. Geological Society, London, Special Publications, 294:279–296.
Schmitt, R.S., Mohriak, W., Mansur, K.L., Skrepnek, C.C., Trouw, R.A.J., Guerra, J.V., Silva, R.S., Ramos, A.S., Stanton, N., Almeida, J.C.H., Heilbron, M., Motoki, A., Sichel, S., Guimarães, P.V., Palermo, N., Silva, F.L., Pereira, R.M., Meneses, P.T., 2009. Mapa Geológico da Folha Rio das Ostras SF.24-Y-A-IV. Belo Horizonte: CPRM, CD-ROM.
Schmitt, R.S., Armstrong, R., 2014. Unraveling the tectonic evolution of Brasiliano orogens from the actual South Atlantic margins – new U-Pb data. In: 9th South American Symposium on Isotope Geology. Program and Abstracts, p. 91.
Schmitt, R.S., Trouw, R., Van Schmus, W.R., Armstrong, R., Stanton, N.S.G., 2016. The tectonic significance of Cabo Frio Tectonic Domain the SE Brazilian margin – a Paleoproterozoic through Cretaceous saga of a reworked continental margin. Braz. J. Geol. 1 (1), 37–66.
Schmitt, R.S., Fragoso, R. de A., Collins, A.S., 2018. Suturing Gondwana in the Cambrian: The Orogenic Events of the Final Amalgamation. In: Siegesmund, S., Basei, M.A.S., Oyhantçabal, P., Oriolo, S. (Eds.), Geology of Southwest Gondwana. Springer International Publishing, Cham, 411–432.
Seth, B., Kröner, A., Mezger, K., Nemchin, A.A., Pidgeon, R.T., Okrusch, M., 1998. Archaean to Neoproterozoic magmatic events in the Kaoko belt of NW Namibia and their geodynamic significance. Precambr. Res. 92 (4), 341–363.
Silva, L.C., Mcnaughton, N.J., Hartmann, L.A., Fletcher, I.R., 2003. Zircon U-Pb SHRIMP dating of the Serra dos Órgãos and Rio de Janeiro gneissic granitic suites: implications for the (560 Ma) Brasiliano. Rev. Brasil. Geoci. 33 (2), 237–244.
Sisson, V.B., Pavlis, T.L., Roeske, S.M., Thorkelson, D.J., 2003. Introduction: An overview of ridge-trench interactions in modern and ancient settings, in Sisson, V.B., et al., eds., Geology of a transpressional orogen developed during ridge-trench interaction along the North Pacific margin: Geological Society of America Special Paper 371, p. 1–18.
Smith, H.A., van Barreiro, B., 1990. Monazite U-Pb dating of staurolite grade metamorphism in pelitic. Contrib. Miner. Petrol. 105, 602–615.
Spear, F.S., 1991. On the interpretation of peak metamorphic temperatures in light of garnet diffusion during cooling. J. Metamorphic Geol. 9, 379–388.
Spear, F.S., Kohn, M.J., Cheney, J.T., 1999. P-T paths from anatectic pelites. Contrib. Miner. Petrol. 134 (1), 17–32.
Stanton, N., Schmitt, R.S., Galdeano, A., Maia, M., Mane, M., 2010. Crustal Structure of the Southeastern Brazilian Margin, Campos Basin, from Aeromagnetic Data: New kinematic constraints. Tectonophysics 490, 15–27.
Steiger, R.H., Jäger, E., 1977. Subcommission on geochronology – convention on use of decay constants in geochronology and cosmochronology. Earth Planet. Sci. Lett. 36, 359–362.
Stern, R.J., 2002. Subduction zones. Rev. Geophys., 40/4: 3–1 to 3–38.
Syracuse, E.M., van Keken, P.E., Abers, G.A., 2010. The global range of subduction zone thermal models. Phys. Earth Planet. Inter. 183 (1–2), 73–90.
Tedeschi, M., Lanari, P., Rubatto, D., Pedrosa-Soares, A., Hermann, J., Dussin, I., Pinheiro, M.A.P., Bouvier, A.S., Baumgartner, L., 2017. Reconstruction of multiple P-T-t stages from retrogressed mafic rocks: Subduction versus collision in the Southern Brasília orogen (SE Brazil). Lithos 294–295, 283–303.
Tomkins, H.S., Powell, R., Ellis, D.J., 2007. The pressure dependence of the zirconium-in-rutile thermometer. J. Metam. Geolol. 25, 703–713.
Treloar, P.J., Palin, R.M., Searle, M.P., 2019. Himalayan Tectonics: A Modern Synthesis. Geological Society, London, Special Publications, p. 483.
Trouw, R.A.J., Heilbron, M., Ribeiro, A., Paciullo, F.V.P., Valeriano, C.M., Almeida, J.C. H., Tupinambá, M., Andreis, R.R., 2000. The central segment of the Ribeira belt. In: Cordani, U.G., Milani, E.J., Thomaz Filho, A., Campos, D.A. (Eds.), Tectonic Evolution of South America. 31th International Geological Congress, Rio de Janeiro, Brazil, 287–310.
Trouw, R.A.J., Peternel, R., Ribeiro, A., Heilbron, M., Vinagre, R., Duffles, P., Trouw, C. C., Fontainha, M., Kussama, H.H., 2013. A new interpretation for the interference zone between the Southern Brasília Belt and the Central Ribeira Belt, SE Brazil. J. S. Am. Earth Sci. 48, 43–57.
Tupinambá, M., Teixeira, W., Heilbron, M., 2012. Evolução tectônica e magmática da Faixa Ribeira entre o Neoproterozoico e o Paleozoico Inferior na Região Serrana do Estado do Rio de Janeiro, Brasil. Anuário do Instituto de Geociências – UFRJ 35 (2), 140–151.
Valeriano, C.M., Tupinambá, M., Simonetti, A., Heilbron, M., Almeida, J., Eirado Silva, L., 2011. U-Pb LA-MC-ICPMS geochronology of Cambro-Ordovician post-collisional granites of the Ribeira Belt, southeast Brazil: terminal Brasiliano magmatism in central Gondwana supercontinent. J. S. Am. Earth Sci. 32 (4), 416–428.
Viana, S.M., Valladares, C.S., Duarte, B.P., 2008. Geoquímica dos ortognaisses do Complexo Região dos Lagos, Araruama-Cabo Frio, Rio de Janeiro, Brasil. Rev. Brasil. Geoci. 27 (1), 111–120.
White, R.W., Powell, R., Holland, T.J.B., 2001. Calculation of partial melting equilibria in the system Na_2O–CaO–K_2O–FeO–MgO–Al_2O_3–SiO_2–H_2O (NCKFMASH). J. Metamorph. Geol. 19, 139–153.
Wiedenbeck, M., Alle, P., Corfu, F., Griffin, W.L., Meier, M., Oberli, F., Von Quadt, A., Roddick, J.C., Spiegel, W., 1995. 3 natural zircon standards for U-Th-Pb, Lu-Hf, trace-element and REE analyses. Geostand. Newsl. 19, 1–2.
Williams, I.S., 2001. Response of detrital zircon and monazite, and their U-Pb isotopic systems, to regional metamorphism and host-rock partial melting, Cooma Complex, southeastern Australia. Aust. J. Earth Sci. 48, 557–580.
Williams, M.L., Jercinovic, M.J., Goncalves, P., 2006. Format and philosophy for collecting, compiling, and reporting microprobe monazite ages. Chem. Geol. 225, 1–15.
Yakymchuk, C., Kirkland, C.L., Clark, C., 2018. Th/U ratios in metamorphic zircon. J. Metamorp. Geol. 36, 715–737.